Control of Dual Motors with Redundancy

Dissertation submitted to
Visvesvaraya National Institute of Technology, Nagpur
in partial fulfilment of requirement for the award of
the degree

Master of Technology
in
Power Electronics and Drives

by

Abhijeet Rajesh Geetey
(MT23PED003)

under the guidance of

Dr. Ashwin Dhabale

Department of Electrical Engineering
Visvesvaraya National Institute of Technology
Nagpur-440010

2024-2025

Control of Dual Motors with Redundancy

Dissertation submitted to
Visvesvaraya National Institute of Technology, Nagpur
in partial fulfilment of requirement for the award of
the degree

Master of Technology
in
Power Electronics and Drives

by

Abhijeet Rajesh Geetey
(MT23PED003)

under the guidance of

Dr. Ashwin Dhabale

Department of Electrical Engineering
Visvesvaraya National Institute of Technology
Nagpur-440010

2024-2025

© Visvesvaraya National Institute of Technology (VNIT) 2025

Department of Electrical Engineering

Visvesvaraya National Institute of Technology, Nagpur

Declaration

I, **Abhijeet Rajesh Geetey,** hereby declare that this dissertation titled **"Control of Dual Motors with Redundancy"**is carried out by me in the Department of Electrical Engineering of Visvesvaraya National Institute of Technology, Nagpur. The work is original and has not been submitted earlier whole or in part for the award of any degree/diploma at this or any other Institution/University.

Abhijeet Rajesh Geetey
Enrolment No. MT23PED003
Date 30/05/2025

Certificate

This is to certify that the dissertation titled **""Control of Dual Motors with Redundancy"** is submitted by **Abhijeet Rajesh Geetey**, in partial fulfillment of the requirements for the award of the degree of **Master of Technology in Power Electronics & Drives, VNIT Nagpur**. The work is comprehensive, complete, and fit for final evaluation.

Dr. B.S. Umre
Head, Department of Electrical Engineering,
VNIT, Nagpur
Date: 30.05.2025

Dr. Ashwin Dhabale
Supervisor, Assistant Professor
Department of Electrical Engineering
VNIT, Nagpur

Department of Electrical Engineering

Visvesvaraya National Institute of Technology, Nagpur

NON-PLAGIARISM CERTIFICATE

This is to certify that the M. Tech. Dissertation titled **"Control of Dual Motors with Redundancy"** submitted by **Abhijeet Rajesh Geetey, Enrolment No. MT23PED003, ID No. 30695** is an original work. The similarity index is identified as 22 % which is within prescribed limits.

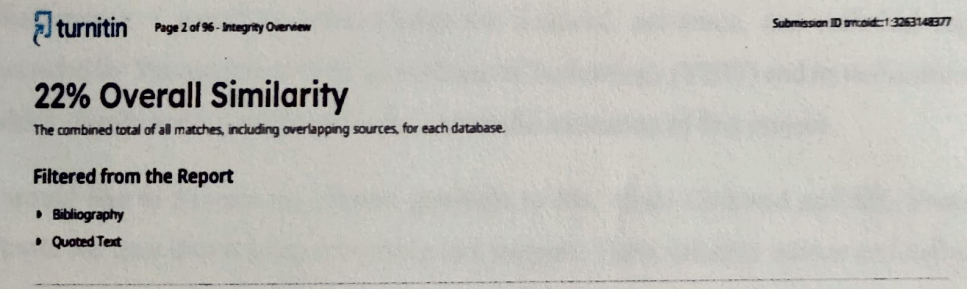
turnitin Page 2 of 96 - Integrity Overview Submission ID trn:oid:::1:3263148377

22% Overall Similarity

The combined total of all matches, including overlapping sources, for each database.

Filtered from the Report

- Bibliography
- Quoted Text

Abhijeet Rajesh Geetey

Enrolment Number: MT23PED003

ID No.: 30695

Date: 30/05/2025

Dr. Ashwin Dhabale

Assistant Professor,

Department of Electrical Engineering,

VNIT, Nagpur

ACKNOWLEDGEMENTS

I would like to express my sincere and heartfelt gratitude to my supervisor, **Dr. Ashwin Dhabale**, for his invaluable guidance, constant encouragement, timely suggestions, and constructive feedback throughout the course of my research. His willingness to clarify my doubts and his continuous support played a crucial role in the successful completion of this work.

I am deeply indebted to **Dr. B. S. Umre**, Professor and Head of the Department of Electrical Engineering at VNIT Nagpur, for his generous assistance and for facilitating financial support for this project. I would also like to extend my appreciation to the officials of VNIT for providing the necessary research infrastructure and facilities.

Furthermore, I gratefully acknowledge the financial, academic, and technical support extended by Visvesvaraya National Institute of Technology (VNIT) and its dedicated staff, which significantly contributed to the successful execution of this project

I would like to express my sincere gratitude to Ms. Nidhi Gaikwad and Mr. Vrundesh Pawde for their unwavering friendship and support. Their valuable advice and insightful suggestions served as a great source of motivation throughout my journey. I am also deeply thankful to research scholar Mr. Mohammad Sajid Sheikh and Ms. Rashmi Singh for their continuous technical support and guidance during the course of my study.

I would like to show my gratitude to my parents Mr. Rajesh Geetey, Mrs Archana Geetey and my sister Ms. Pratha Geetey who showered constant love and support on me.

Finally, I owe my gratitude to my friends, and classmates for their occasional support, suggestions, and help in making this project a success.

ABSTRACT

In modern industrial automation and electric drive systems, the demand for efficient, high-performance, and cost-effective multi-motor solutions has grown significantly. Traditional approaches to powering multiple three-phase induction machines often require complex configurations with a high number of power electronic components, leading to increased system costs and reduced reliability. This research addresses these challenges by proposing an innovative method for driving two three-phase induction machines using a single five-phase power supply, offering improved torque performance and operational efficiency compared to conventional balanced five-phase systems.

The study focuses on developing a novel control scheme that enables smooth torque output while maintaining independent control over each machine—a critical requirement for industrial applications where precision and reliability are paramount. Transforming the equations of both machines into the stationary reference frame allows them to be analysed independently of one another. A comprehensive Simulink model is developed to simulate and analyse the performance of this approach under various operating conditions. The simulation results of the proposed model show that, unlike the conventional approach which requires two three-leg inverters to run two three-phase induction motors, this model operates both motors using a single five-leg inverter (FLI). This demonstrates reduced hardware redundancy, as one inverter leg is eliminated without affecting performance.

Additionally, the research identifies and discusses the key conditions necessary to achieve simultaneous independent control and ripple-free torque operation. These findings provide valuable guidelines for designing more compact, economical, and high-performance multi-motor drive systems. The outcomes of this study have significant implications for industrial applications, particularly in sectors such as manufacturing, robotics, and electric transportation, where efficient multi-motor control is essential. Future work could explore fault-tolerant designs and scalability to larger systems, further advancing the practicality and adoption of multi-phase drive technologies.

LIST OF FIGURES

Figure 2.1(a) and 2.1(b) shows the d-axis and the q-axis currents of the motor at no load 15

Figure 2.2 shows the three phase currents of the motor for free acceleration at no load 15

Figure 2.3 shows the Electromagnetic Torque of the motor for free acceleration at no load 16

Figure 2.4 shows Speed (RPM) of the motor for free acceleration at no load..... 16

Figure 2.5 shows the torque v/s speed of the motor for free acceleration at no load 17

Figure 2.6(a) and 2.6(b) shows the d-axis and the q-axis currents of the motor at rated load 18

Figure 2.7 shows the three phase currents of the motor for free acceleration at Rated load 19

Figure 2.8 shows torque of the motor for free acceleration at rated load 19

Figure 2.9 shows Speed (RPM) of the motor for free acceleration at rated load..... 19

Figure 2.10 shows Torque vs Speed of the motor for free acceleration at rated load 20

Figure 3.1 Conventional three-phase two-level voltage source inverter with balanced load 23

Figure 3.2: Schematic diagram of SVPWM 29

Figure 3.3 Vector diagram of SVPWM..... 30

Figure 3.4 Algorithm of sector determination..... 31

Figure 3.5 Sector 1 calculation diagram 32

Figure 4.1: Block diagram of the open loop Volts/Hz control for an induction motor 38

Figure 4.2: Phasor Diagram of Vector Controller..... 42

Figure 4.3: Implementation of the indirect vector control..... 46

Figure 4.4: Simulation Results of FOC 47

Figure 5.1 Block Diagram for The Proposed Scheme 50

Figure 5.2 Five Phase balanced supply 51

Figure 5.3 Waveform of five phase supply 52

Figure 5.4 (a) RMF of actual ACE 52

Figure 5.4(b) RMF of actual ABD 52

Figure 5.5 Balanced three phase winding supplied from ACE 53

Figure 5.6 (a) RMF of Modified ACE 55

Figure 5.6 (b) RMF of Modified ABD 55

Figure 5.8 Alpha, Beta and Zero Voltages 56

Figure (5.9(A)) Balanced Supply for Motor 1 57

Figure (5.9(B)) Supply of Motor 2 Which Can Be Balanced as Well as Unbalanced 57

Figure 5.10 (a) (i)Phase Voltages (ii)V_{alpha},V_{beta} and V_{zero} (iii)RMF of Motor 1 and Motor 2 respectively when A=0.75 59

Figure 5.10 (b) (i)Phase Voltages (ii)V_{alpha},V_{beta} and V_{zero} (iii)RMF of Motor 1 and Motor 2 respectively when A=0.5 60

Figure 5.10 (c) (i)Phase Voltages (ii)V_{alpha},V_{beta} and V_{zero} (iii)RMF of Motor 1 and Motor 2 respectively when A=0.65 61

Figure 5.10 (d) (i)Phase Voltages (ii)V_{alpha},V_{beta} and V_{zero} (iii)RMF of Motor 1 and Motor 2 respectively when A=0.85 62

Fig. 5.10 (e) (i)Phase Voltages (ii)V_{alpha},V_{beta} and V_{zero} (iii)RMF of Motor 1 and Motor 2 respectively when A=1 63

Figure 5.11 Stator Flux Vs Rotor Flux in Stationary Reference Frame 64

LIST OF TABLES

Table.2.1 Parameters of Three Phase Induction Motor 14

Table 3.1 Switching Combinations and Normalized Output Voltages for a Three-Phase Two-Level Inverter 24

Table 3.2 $\alpha\beta$ Frame Representation of Switching Vectors for a Three-Phase Two-Level Inverter 27

Table3.3 Dwell Time of Switching and Every Sector 35

Table 4.1: Parameters of Three Phase Induction Motor (50 Hp)..... 46

NOTATIONS AND ABBREVIATION

IM	Induction Motor
FLI	Five Leg Inverter
PWM	Pulse Width Modulation
SVPWM	Space Vector PWM
SPWM	Sinusoidal PWM
FOC	Field Oriented Control
DTC	Direct Torque Control
VSI	Voltage Source Inverter
RES	Renewable Energy Systems
AC	Alternating Current
g	Gain Factor
A	Voltage magnitude of motor 1
B	Voltage magnitude of motor 2
DC	Direct Current
VFD	Variable Frequency Drives
f	Frequency (Hz)
ω	Frequency(rad)
R	Resistance
L	Inductance
X	Reactance
p	Derivative
P	Poles
d	Direct axis
q	Quadrature axis
s	Stator reference frame
e	Synchronous reference frame
r	Rotor reference frame
c	Arbitrary reference frame
$\mathbf{T_e}$	Electromagnetic Torque
$\mathbf{T_L}$	Load Torque

B	Friction coefficient
J	Moment of inertia
Hp	Horse power
W	Watt
Hz	Hertz
Θ	Angles in Radians
°	degrees
Ω	Ohm
Kg	Kilogram
N	newton
m	meter
RMF	Rotating Magnetic Field

Contents

ABSTRACT ..... **vi**

LIST OF FIGURES ..... **vii**

LIST OF TABLES ..... **ix**

CHAPTER 1 ..... **2**

INTRODUCTION **2**

1.1 Background **2**

1.2 Literature Survey **4**

1.3 Problem Statement **6**

1.4 Thesis Outline **7**

CHAPTER 2 ..... **9**

DYNAMIC MODELLING OF THREE PHASE INDUCTION MOTOR **9**

2.1 Introduction **9**

2.2 Generalized Model in Arbitrary Reference Frame **10**

2.3 Stator Reference Frame **11**

2.4 Rotor Reference Frame **11**

2.5 Synchronous Reference Frame **12**

2.5.1 Solution of The Differential Equation 13

2.6 Free Acceleration Characteristics **14**

2.6.1. At No Load: (Results and Observations) 14

2.6.2 At Rated Load 17

CHAPTER 3 ..... **22**

SPACE VECTOR PULSE WIDTH MODULATION 22

3.1 Introduction of SVPWM 22

3.2 Switching states of a three phase two level inverter 23

3.3 Clarke and Park Transformation **25**

3.4 Steps for Implementing SVPWM Technique 3Φ Two-Level VSI .. **29**

3.6 Conclusion: **35**

CHAPTER 4 ..... **37**

CONTROL SCHEME FOR INDUCTION MOTOR DRIVES **37**

4.1 Introduction **37**

4.2 Scalar Control of Induction Machine **37**

4.2.1 Open Loop Volts/Hz Control 37

4.3 Vector Control of Induction Motor **40**

4.3.1 Principle of Vector Control 41

4.3.2 Derivation of Indirect Vector Control for Induction Motor 43

4.3.3. Implementation Of Indirect Vector Control 45

4.4 Results and Observations: **47**

CHAPTER 5 ..... **50**

CONTROL OF DUAL MOTORS WITH REDUNDANCY **50**

5.1 Introduction: **50**

5.2 Balanced Five Phase Supply: **51**

5.3 Different Set of Phases **56**

5.4 Deriving B, Θ_b and Θ_c in terms of A **57**

5.5 Results and Conclusion: **59**

5.5.1Case 1: When A=B=0.75 then $\boldsymbol{\theta b = 120°}$ and $\boldsymbol{\theta c = -120°}$ 59

5.5.2 Case 2: When A= 0.5 then B=0.9017, $\boldsymbol{\theta b = 133.87°}$ and $\boldsymbol{\theta c = -133.87°}$ 60

5.5.3 Case 3: When A= 0.65 then B=0.8050, $\boldsymbol{\theta b = 126.158°}$ and $\boldsymbol{\theta c = -126.158°}$ 61

5.5.4 Case 4: When A= 0.85 then B=0.70578, $\boldsymbol{\theta b = 112.932°}$ and $\boldsymbol{\theta c = -112.932°}$ 62

5.5.5 Case 5: When A= 1 then B=0.6619, $\boldsymbol{\theta b = 100.8855°}$ and $\boldsymbol{\theta c = -100.8855°}$ 63

CHAPTER-6 ..... **67**

CONCLUSION AND FUTURE SCOPE 67

6.1 Conclusion..... 67

6.2 Future Scope 68

REFERENCES..... 69

Chapter 1

INTRODUCTION

CHAPTER 1

INTRODUCTION

1.1 Background

Electric motors form the foundation of modern automation and electrification, powering applications ranging from conveyor belts and robotic manipulators to electric vehicles and smart manufacturing systems. As industries increasingly adopt flexible and intelligent automation strategies, the need for efficient, compact, and cost-effective motor control solutions has become paramount. Choosing the right motor and control strategy depends on understanding the characteristics of both the machine and the control methodology.

Historically, DC motors particularly brushed DC and permanent magnet synchronous variants were preferred for precise speed and torque control due to their simple dynamics and fast transient response. These motors provided excellent controllability, making them ideal for servo and feedback-driven systems. However, brushed DC motors suffered from limitations such as brush wear, frequent maintenance, and the potential for spark generation in hazardous environments [1]. Although DC permanent magnet synchronous motors (PMSMs) addressed some of these concerns by eliminating the brush-commutator assembly, they introduced their own challenges: increased rotor inertia, mechanical complexity, and higher costs, particularly in high-power or high-speed applications [2].

The development of advanced power electronics and control theory marked a major turning point. In the 1960s, the concept of vector control also known as Indirect Field-Oriented Control (IFOC) was introduced to enable dynamic control of AC induction machines [3]. While early implementations faced challenges due to limited computational capability and sensor technologies, the emergence of high-speed digital signal processors (DSPs), insulated-gate bipolar transistor (IGBT)-based inverters, and precision rotor position sensors has made real-time vector control practical and efficient [4].

Vector control transforms the stator currents of an AC machine into a rotating reference frame, allowing the independent regulation of torque and flux. This is achieved by decoupling the stator current into two orthogonal components: the direct axis current (I_d), responsible for flux generation, and the quadrature axis current (I_q), which produces torque [3]. This decoupling makes the dynamic behaviour of AC induction motors comparable to that of separately excited DC motors, but with the benefits of robustness, low maintenance, and cost-effective construction. Moreover, unlike permanent magnet machines that rely on fixed rotor flux, induction motors allow dynamic control of rotor flux, offering greater flexibility in high-performance applications [5].

As control capabilities matured, the industrial landscape evolved to include increasingly complex systems involving multiple electric drives. In sectors such as textile processing, robotics, electric traction, and material handling, the need for multi-motor coordination became evident. Traditionally, each motor in such systems is driven by its own three-phase inverter connected to a common DC link, allowing for independent vector or direct torque control using Clarke and Park transformations. However, this arrangement scales poorly: each motor demands three inverter legs, resulting in bulky and expensive hardware configurations as the number of motors increases [6], [7].

To address this, novel inverter and machine configurations have been explored, aiming to reduce the number of components without compromising control performance. This thesis investigates one such approach: the use of multiphase drive systems to control multiple motors with a reduced number of inverter legs. A key insight is that, for any *n*-phase machine, only two current components are needed to independently regulate torque and flux. The remaining degrees of freedom can be harnessed to control additional machines within the same system [8], [9].

By leveraging this principle, a five-phase voltage source inverter (VSI) can be designed to independently control two standard three-phase induction motors each with full vector control capability. Unlike earlier strategies that relied on series interconnection of stator windings and precise phase transpositions often resulting in fragility and susceptibility to single-point failures this approach maintains complete electrical independence between the motors. It eliminates the need for complex winding

arrangements, improving reliability, simplifying hardware design, and enhancing fault tolerance [10], [11].

Furthermore, this configuration benefits from the use of generalized transformation matrices that eliminate the need for real-time trigonometric calculations, reducing computational load on the DSP and improving efficiency. The five-phase architecture also enables the exploitation of third spatial harmonic components to boost torque density, further enhancing performance [12], [13].

Experimental validation confirms that such systems achieve excellent dynamic behaviour, including accurate speed tracking, smooth torque response, and effective decoupling between the controlled motors. A generalized principle has emerged from related work: an *n*-phase inverter can independently control up to (n−1)/2 three-phase machines, offering a scalable and resource-efficient architecture for modern industrial applications [8], [10].

In this thesis, a novel vector control system is proposed and experimentally demonstrated, wherein two independent three-phase induction motors are driven by a single five-phase VSI. The system avoids traditional constraints such as series interconnection and phase transposition, while achieving robust, decoupled control for each motor. The successful implementation not only confirms theoretical predictions but also points toward a promising direction for high-performance, space-efficient, and cost-effective multi-motor drive systems in next-generation industrial environments.

1.2 Literature Survey

The evolution of electric motor drives has been extensively studied over the past several decades. Traditional systems relied on DC machines due to their inherent ease of control and linear torque-speed characteristics. However, their mechanical limitations and maintenance requirements eventually led to a shift towards AC induction motors [1], [2]. Early control strategies for induction machines were largely scalar in nature, emphasizing simplicity over dynamic performance. These included Volts-per-Hertz (V/f) methods, which were adequate for constant speed applications but inadequate for dynamic environments [3].

A breakthrough came with the development of Indirect Field-Oriented Control (IFOC) by Blaschke and Hasse in the early 1970s [3]. IFOC allowed for the decoupled control of torque and flux in AC machines by transforming stator currents into a rotating reference frame using Clarke and Park transformations. This transformation enabled AC machines to emulate the dynamic characteristics of DC motors. Despite its theoretical promise, the widespread adoption of vector control was delayed due to the computational complexity and lack of suitable real-time hardware at the time [4].

The rapid advancement in digital signal processors (DSPs), IGBT-based inverters, and high-resolution position encoders eventually overcame these limitations, making real-time vector control practical and commercially viable [4], [5]. Modern vector control systems now offer precise speed and torque control, high efficiency, and smooth transient responses across wide operating ranges.

Parallel to this, the demand for multi-motor systems grew in industrial sectors such as robotics, transportation, and automated manufacturing. These systems typically used separate inverters for each motor, interconnected by a common DC link. While this approach allowed for independent control, it significantly increased the overall cost, complexity, and size of the drive system [6], [7].

In response to this, research began focusing on multiphase drive systems, which use inverters with more than three phases to control multiple machines. A central theoretical insight, established in works like [8] and [9], is that in an *n*-phase system, only two current components are needed for independent control of torque and flux. The additional degrees of freedom can be exploited to control extra machines without interference, significantly reducing hardware requirements.

One practical implementation involves using a five-phase voltage source inverter (VSI) to drive two three-phase induction motors independently. Initial configurations used series or parallel connections of stator windings, which required exact phase alignment and increased system vulnerability to single-point failures [10]. These designs often suffered from reliability issues and lacked the modularity desired in industrial settings.

To address these challenges, more recent works have explored topologies that avoid series interconnection, allowing each motor to retain electrical and control independence while sharing the same inverter [11], [12]. This avoids cascading faults, reduces wiring complexity, and simplifies system protection schemes. In particular, the work in [13] demonstrates the feasibility of controlling two standard three-phase machines using a five-phase inverter, enabled by carefully designed modulation and transformation strategies.

Further innovations have included the use of generalized Clarke and Park transformations for multiphase systems, which allow control algorithms to be implemented efficiently without relying on computationally intensive trigonometric operations [12]. This is especially valuable for DSP-based control platforms where computational resources are limited. Additionally, studies such as [14] and [15] have shown that multiphase machines, particularly five-phase motors, can exploit third harmonic components to increase torque density and reduce torque ripple, making them attractive for high-performance applications.

Despite these advancements, practical implementation remains a critical area of study Many theoretical models assume ideal conditions and perfect parameter matching, which may not be achievable in real-world environments. The work presented in [8], [10], and [13] lays important groundwork, but there remains a need for experimental validation under realistic conditions, especially using standard, commercially available induction motors and minimal hardware modifications.

1.3 Problem Statement

The primary objective of this project is to develop an advanced control strategy that facilitates the independent operation of two three-phase induction motors using a five-phase inverter-based drive system. The novelty lies in the efficient utilization of a higher-phase inverter (five-phase) to control multiple standard three-phase machines, reducing hardware complexity while optimizing performance. However, this configuration introduces critical technical challenges that must be addressed for practical viability and robust performance. This involves addressing two primary technical challenges:

1. Mitigation of torque oscillations, which are typically exacerbated when both machines are simultaneously fed from a five-phase source, leading to undesirable torsional effects.

2. Decoupled control of the individual motors, ensuring that each machine can be regulated independently in terms of speed and torque, despite being driven by the same supply system.

3. Considering first three legs of FLI as 3 phase VSI and generating phase difference in other two legs in such a way that it also gives balanced supply without complex circuitry.

4. Input for the Motor is Voltage and Frequency and the output is Torque and Speed, so to analyze the dependency of the two motors on these four parameters in order to make both independent of each other.

1.4 Thesis Outline

Chapter 1 provides a brief introduction of the project discussing the problem statement along with the literature survey carried out.

Chapter 2 discusses SVPWM in detail, explaining its working principle with the help of schematic diagrams, vector representation, and switching strategies.

Chapter 3 discusses the dynamic modelling of a three-phase induction motor, presenting the mathematical formulation and highlighting the results obtained from the model.

Chapter 4 provides an overview of various control schemes for the three-phase induction motor, including scalar control(V/f), vector control (FOC), and Direct Torque Control (DTC). While the theoretical background of each method is discussed, the chapter primarily presents the results obtained from implementing the FOC technique.

Chapter 5 explains the proposed work outlining the approach with the help of schematic diagrams, relevant equations, and waveforms results to demonstrate its effectiveness.

Chapter 6 presents the conclusion of the work carried out and outlines the future scope for further development and research.

Chapter 2

MODELLING OF THREE PHASE INDUCTION MOTOR

CHAPTER 2

DYNAMIC MODELLING OF THREE PHASE INDUCTION MOTOR

2.1 Introduction

The steady-state model and its equivalent circuits are useful for studying the performance of the machine in steady state. This implies that all electrical transients are neglected during load changes and stator frequency variations. Such variations arise in applications involving variable-speed drives. The variable-speed drives are converter-fed from finite sources, unlike the utility sources, due to the limitations of the switch ratings and filter sizes. This results in their incapability to supply large transient power. Hence, we need to evaluate the dynamics of converter-fed variable-speed drives to assess the adequacy of the converter switches and the converters for a given motor and their interaction to determine the excursions of currents and torque in the converter and motor. The dynamic model considers the instantaneous effects of varying voltages/currents, stator frequency, and torque disturbance. The dynamic model of the induction motor is derived by using a two-phase motor in direct and quadrature axes. This approach is desirable because of the conceptual simplicity obtained with two sets of windings, one on the stator and the other on the rotor. The reference frames are chosen to be arbitrary and particular cases such as stationery, rotor and synchronous reference frames are simple instances of the general case. The differential equations describing the dynamics of the induction motor are nonlinear. For stability and controller design studies, it is important to linearize the machine equations around a steady - state operating point to obtain the small - signal equations.

The following assumptions are generally made to derive the dynamic model of the induction motor.

1. Uniform air gap

2. Balanced rotor and stator windings with sinusoidally distributed mmf

3. Inductance vs rotor position is sinusoidal

4. Saturation and parameter changes are neglected

2.2 Generalized Model in Arbitrary Reference Frame

Reference frames rotating at an arbitrary speed are hereafter called arbitrary reference frames. Other reference frames are particular cases of these arbitrary reference frames. From now on, the three-phase machine is assumed to have balanced windings and balanced inputs, thus eliminating the zero sequence equations from further consideration. Note that the zero-sequence equations have to be included only for unbalanced operation of the motor, a situation common with a fault in the machine or converter.

The induction motor model in arbitrary reference frame is given by:

$$v_{qs}^{c} = (R_s + L_s p) i_{qs}^{c} + \omega_c L_s i_{ds}^{c} + L_m p i_{qr}^{c} + \omega_c L_m i_{dr}^{c} \tag{2.1}$$

$$v_{ds}^{c} = -\omega_c L_s i_{qs}^{c} + (R_s + L_s p) i_{ds}^{c} - \omega_c L_m i_{qr}^{c} + L_m p i_{dr}^{c} \tag{2.2}$$

$$v_{qr}^{c} = L_m p i_{qs}^{c} + (\omega_c - \omega_r) L_m i_{ds}^{c} + (R_r + L_r p) i_{qr}^{c} + (\omega_c - \omega_r) L_r i_{dr}^{c} \tag{2.3}$$

$$v_{dr}^{c} = -(\omega_c - \omega_r) L_m i_{qs}^{c} + L_m p i_{ds}^{c} - (\omega_c - \omega_r) L_r i_{qr}^{c} + (R_r + L_r p) i_{dr}^{c} \tag{2.4}$$

Which could be written in matrix form as:

$$\begin{bmatrix} v_{qs}^{c} \\ v_{ds}^{c} \\ v_{qr}^{c} \\ v_{dr}^{c} \end{bmatrix} = \begin{bmatrix} R_s + L_s p & \omega_c L_s & L_m p & \omega_c L_m \\ -\omega_c L_s & R_s + L_s p & -\omega_c L_m & L_m p \\ L_m p & (\omega_c - \omega_r) L_m & R_r + L_r p & (\omega_c - \omega_r) L_r \\ -(\omega_c - \omega_r) L_m & L_m p & -(\omega_c - \omega_r) L_r & R_r + L_r p \end{bmatrix} \begin{bmatrix} i_{qs}^{c} \\ i_{ds}^{c} \\ i_{qr}^{c} \\ i_{dr}^{c} \end{bmatrix}$$

Where 'c' denotes arbitrary reference frame and ω_c represents the speed of the reference frame. The electromagnetic torque developed by the motor is given by:

$$T_e = \frac{3}{2}\frac{P}{2} L_m \left(i_{qs}^{c} i_{dr}^{c} - i_{ds}^{c} i_{qr}^{c} \right) \tag{2.5}$$

The electro-mechanical torque equation is

$$T_e = J \frac{2}{P} \frac{d\omega_r}{dt} + B \frac{2}{p} \omega_r + T_L \tag{2.6}$$

2.3 Stator Reference Frame

Since the reference is stationary, the angular velocity of the reference frame would be

$$\omega_c = 0 \tag{2.7}$$

hence the equations become:

$$v_{qs} = (R_s + L_s p)i_{qs} + L_m p i_{qr} \tag{2.8}$$

$$v_{ds} = (R_s + L_s p)i_{ds} + L_m p i_{dr} \tag{2.9}$$

$$v_{qr} = L_m p i_{qs} - \omega_r L_m i_{ds} + (R_r + L_r p)i_{qr} - \omega_r L_r i_{dr} \tag{2.10}$$

$$v_{dr} = \omega_r L_m i_{qs} + L_m p i_{ds} + \omega_r L_r i_{qr} + (R_r + L_r p)i_{dr} \tag{2.11}$$

Which could be written in matrix form as:

$$\begin{bmatrix} v_{qs} \\ v_{ds} \\ v_{qr} \\ v_{dr} \end{bmatrix} = \begin{bmatrix} R_s + L_s p & 0 & L_m p & 0 \\ 0 & R_s + L_s p & -\omega_c L_m & L_m p \\ L_m p & -\omega_r L_m & R_r + L_r p & -\omega_r L_r \\ \omega_r L_m & L_m p & \omega_r L_r & R_r + L_r p \end{bmatrix} \begin{bmatrix} i_{qs} \\ i_{ds} \\ i_{qr} \\ i_{dr} \end{bmatrix}$$

The electromagnetic torque developed by the motor is given by:

$$T_e = \frac{3}{2}\frac{P}{2} L_m \left(i_{qs} i_{dr} - i_{ds} i_{qr}\right) \tag{2.12}$$

2.4 Rotor Reference Frame

The reference is with rotor which is rotating at a speed of ω_r.

$$\omega_c = \omega_r \tag{2.13}$$

hence the equations become:

$$v_{qs}^r = (R_s + L_s p)i_{qs}^r + \omega_r L_s i_{ds}^r + L_m p i_{qr}^r + \omega_r L_m i_{dr}^r \tag{2.14}$$

$$v_{ds}^r = -\omega_r L_s i_{qs}^r + (R_s + L_s p)i_{ds}^r - \omega_r L_m i_{qr}^r + L_m p i_{dr}^r \tag{2.15}$$

$$v_{qr}^r = L_m p i_{qs}^r + (R_r + L_r p)i_{qr}^r \tag{2.16}$$

$$v_{dr}^r = L_m p i_{ds}^r + (R_r + L_r p)i_{dr}^r \tag{2.17}$$

Which could be written in matrix form as:

$$\begin{bmatrix} v_{qs}^r \\ v_{ds}^r \\ v_{qr}^r \\ v_{dr}^r \end{bmatrix} = \begin{bmatrix} R_s + L_s p & \omega_r L_s & L_m p & \omega_r L_m \\ -\omega_r L_s & R_s + L_s p & -\omega_r L_m & L_m p \\ L_m p & 0 & R_r + L_r p & 0 \\ 0 & L_m p & 0 & R_r + L_r p \end{bmatrix} \begin{bmatrix} i_{qs}^r \\ i_{ds}^r \\ i_{qr}^r \\ i_{dr}^r \end{bmatrix}$$

Where 'r' denotes rotor reference frame. The electromagnetic torque developed by the motor is given by:

$$T_e = \frac{3}{2}\frac{P}{2} L_m \left(i_{qs}^r i_{dr}^r - i_{ds}^r i_{qr}^r \right) \tag{2.18}$$

2.5 Synchronous Reference Frame

Reference is rotating with synchronous speed for this case.

$$\omega_c = \omega_s \tag{2.19}$$

$$v_{qs}^s = (R_s + L_s p) i_{qs}^s + \omega_s L_s i_{ds}^s + L_m p i_{qr}^s + \omega_s L_m i_{dr}^s \tag{2.20}$$

$$v_{ds}^c = -\omega_s L_s i_{qs}^s + (R_s + L_s p) i_{ds}^s - \omega_s L_m i_{qr}^s + L_m p i_{dr}^s \tag{2.21}$$

$$v_{qr}^s = L_m p i_{qs}^s + (\omega_s - \omega_r) L_m i_{ds}^s + (R_r + L_r p) i_{qr}^s + (\omega_s - \omega_r) L_r i_{dr}^s \tag{2.22}$$

$$v_{dr}^s = -(\omega_s - \omega_r) L_m i_{qs}^s + L_m p i_{ds}^s - (\omega_s - \omega_r) L_r i_{qr}^s + (R_r + L_r p) i_{dr}^s \tag{2.23}$$

Which could be written in matrix form as:

$$\begin{bmatrix} v_{qs}^s \\ v_{ds}^s \\ v_{qr}^s \\ v_{dr}^s \end{bmatrix} = \begin{bmatrix} R_s + L_s p & \omega_s L_s & L_m p & \omega_s L_m \\ -\omega_s L_s & R_s + L_s p & -\omega_s L_m & L_m p \\ L_m p & (\omega_s - \omega_r) L_m & R_r + L_r p & (\omega_s - \omega_r) L_r \\ -(\omega_s - \omega_r) L_m & L_m p & -(\omega_s - \omega_r) L_r & R_r + L_r p \end{bmatrix} \begin{bmatrix} i_{qs}^s \\ i_{ds}^s \\ i_{qr}^s \\ i_{dr}^s \end{bmatrix}$$

Where the superscript 's' denotes synchronous reference frame. The electromagnetic torque developed by the motor is given by:

$$T_e = \frac{3}{2}\frac{P}{2} L_m \left(i_{qs}^s i_{dr}^s - i_{ds}^s i_{qr}^s \right) \tag{2.24}$$

We use squirrel cage induction motor in our design and hence, v_{qr}^{s} and v_{dr}^{s} are zero. For synchronously rotating machine, we get a DC voltage equivalent to the peak phase voltage, on d-axis, and the q-axis voltage remains zero at all instances. Hence, the matrix could be written as:

$$\begin{bmatrix} 0 \\ v_p \\ 0 \\ 0 \end{bmatrix} = \begin{bmatrix} R_s + L_s p & \omega_s L_s & L_m p & \omega_s L_m \\ -\omega_s L_s & R_s + L_s p & -\omega_s L_m & L_m p \\ L_m p & (\omega_s - \omega_r) L_m & R_r + L_r p & (\omega_s - \omega_r) L_r \\ -(\omega_s - \omega_r) L_m & L_m p & -(\omega_s - \omega_r) L_r & R_r + L_r p \end{bmatrix} \begin{bmatrix} i_{qs}^{s} \\ i_{ds}^{s} \\ i_{qr}^{s} \\ i_{dr}^{s} \end{bmatrix}$$

2.5.1 Solution of The Differential Equation

We prefer to use synchronously rotating reference frame for further analysis and linearization. Eqn.2.20 and Eqn.2.22 have two current derivative components in q axis while Eqn.2.21 and Eqn.2.23 have two current derivative components in d axis. By simply solving these equations, we get

$$p\begin{bmatrix} i_{qs} \\ i_{ds} \\ i_{qr} \\ i_{dr} \end{bmatrix} = \frac{1}{D}\left(\begin{bmatrix} -\omega_s R_s X_r & -\omega_s D - \omega_r X_m^2 & \omega_s R_r X_m & -\omega_r X_m X_r \\ \omega_s D + \omega_r X_m^2 & -\omega_s R_s X_r & \omega_r X_m X_r & \omega_s R_r X_m \\ \omega_s R_s X_m & \omega_r X_m X_s & -\omega_s R_r X_s & -\omega_s D + \omega_r X_s X_r \\ \omega_r X_m X_s & -\omega_s R_s X_m & \omega_s D - \omega_r X_s X_r & -\omega_s R_r X_s \end{bmatrix} \begin{bmatrix} i_{qs} \\ i_{ds} \\ i_{qr} \\ i_{dr} \end{bmatrix} + \begin{bmatrix} \omega_s X_r & 0 & -\omega_s X_m & 0 \\ 0 & \omega_s X_r & 0 & -\omega_s X_m \\ -\omega_s X_m & 0 & \omega_s X_s & 0 \\ 0 & -\omega_s X_m & 0 & \omega_s X_s \end{bmatrix} \begin{bmatrix} v_{qs} \\ v_{ds} \\ v_{qr} \\ v_{dr} \end{bmatrix} \right)$$

Where $D = X_s X_r - X_m^2$

By solving Eqn.2.6 after substituting T_e from Eqn.2.5 into it, we get,

$$\dot{\omega}_r = \frac{3P^2 X_m}{8J\omega_s}\left(i_{qs} i_{dr} - i_{ds} i_{qr}\right) - \frac{B\omega_r}{J} - \frac{PT_L}{2J} \qquad (2.25)$$

These five equations together form the non-linear differential equation of a three-phase induction motor in synchronous reference frame.

2.6 Free Acceleration Characteristics

Table.2.1 Parameters of Three Phase Induction Motor

Power	**5 Hp**
Poles	**4**
Voltage	**200 V**
Frequency(f)	**60 Hz**
R_s	**0.183 Ω**
R_r	**0.277 Ω**
L_s	**0.0553 H**
L_r	**0.056 H**
L_m	**0.0538 H**
J	**0.0165 kg-m^2**
T_L	**10 Nm**

The main understanding of a model is obtained by observing the variables during free acceleration from stand still condition to steady state condition. The motor is initially at rest (at t=0), and then it accelerates freely, to reach the steady state rated speed. The details and specifications of the motor used here, is given below

2.6.1. At No Load: (Results and Observations)

Here we consider that the motor starts freely from rest, without load and it gains speed gradually by free acceleration and attains desired steady state operation at 1800rpm. Fig. 2.1(a) and 2.1(b) shows the d-axis and the q-axis currents of the motor for this period. Fig. 2.2 shows the three phase currents of the motor for free acceleration at no load. Motor torque increases rapidly for starting the free acceleration and then gradually comes down to load torque, which is zero in this case, and this is depicted in Fig. 2.3. Since the motor is initially at standstill, it starts with zero speed and reaches rated speed at steady state, as

shown in Fig. 2.4. speed-torque characteristic of motor during this time is shown Fig 2.5

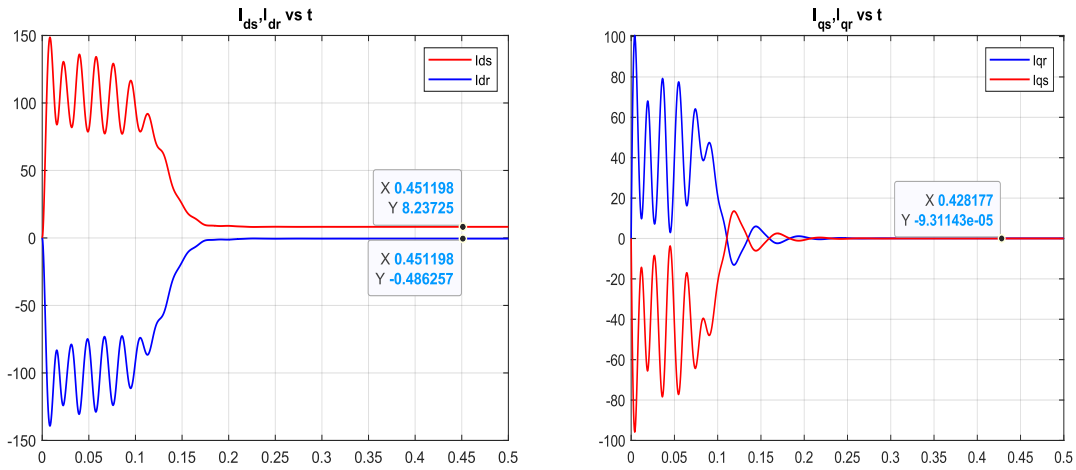

Figure 2.1(a) and 2.1(b) shows the d-axis and the q-axis currents of the motor at no load

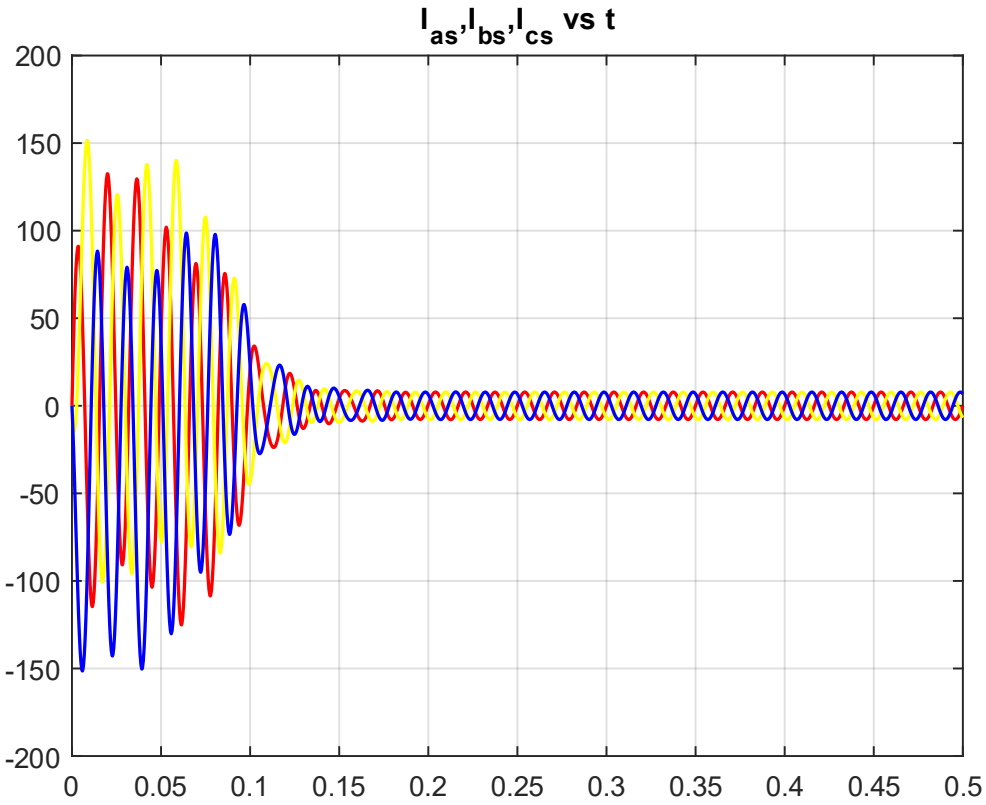

Figure 2.2 shows the three phase currents of the motor for free acceleration at no load

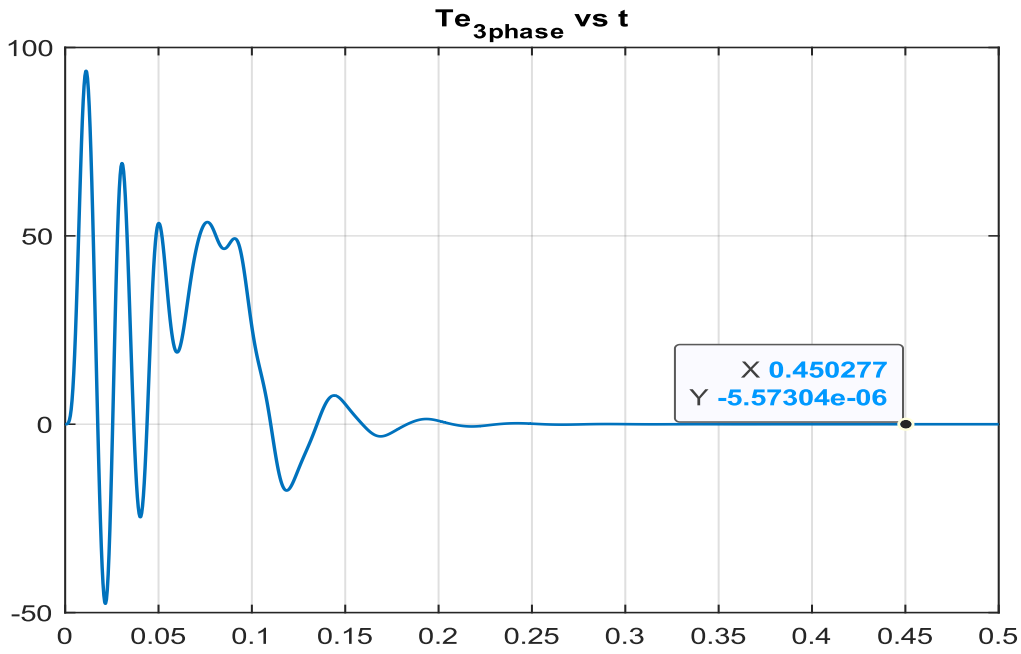

Figure 2.3 shows the Electromagnetic Torque of the motor for free acceleration at no load

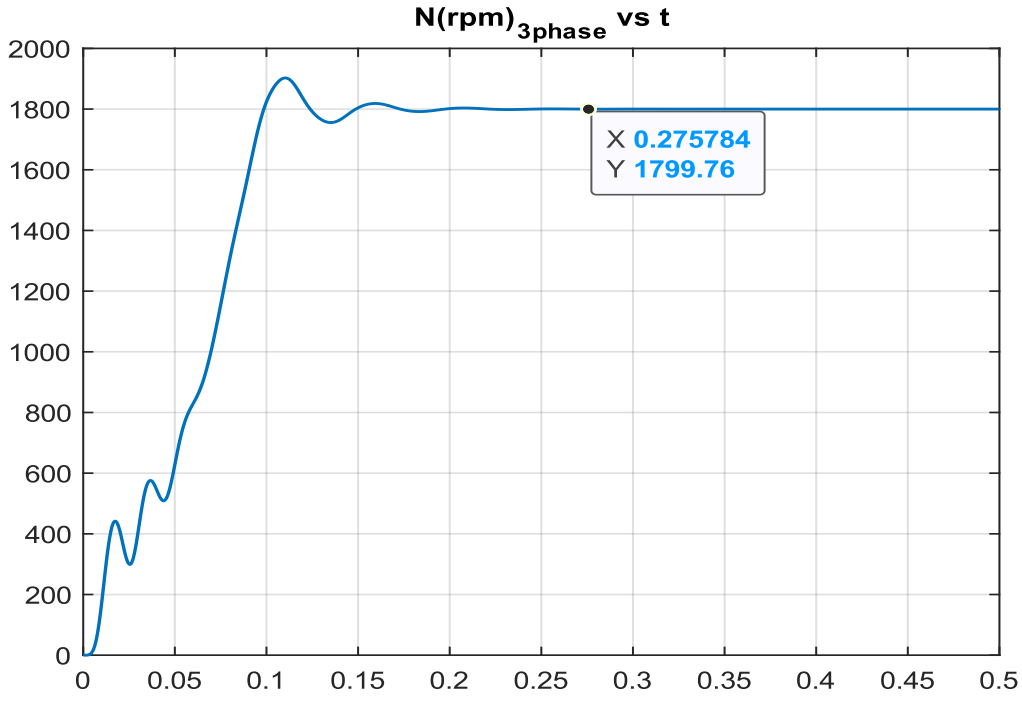

Figure 2.4 shows Speed (RPM) of the motor for free acceleration at no load

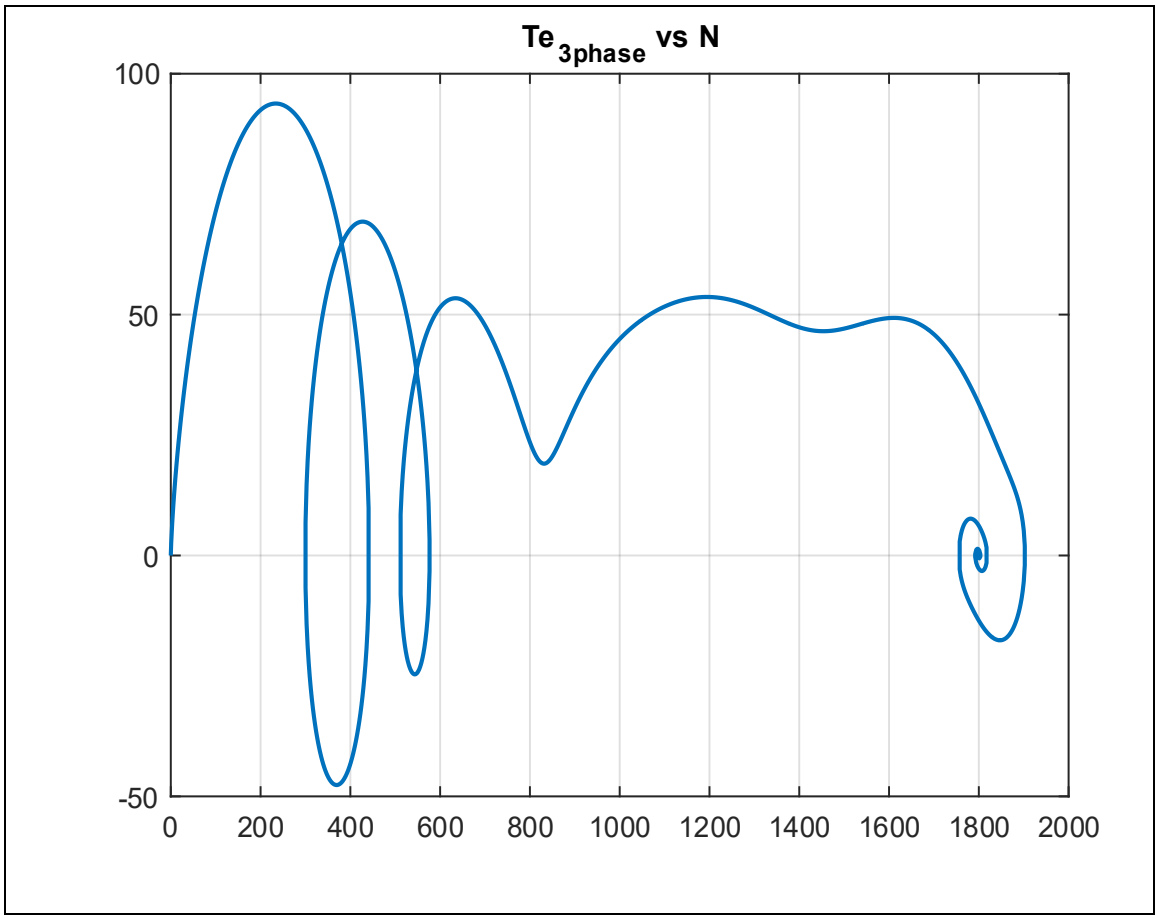

Figure 2.5 shows the torque v/s speed of the motor for free acceleration at no load

2.6.2 At Rated Load

In this section we discuss the response of the motor when it starts from rest and attains steady state values, while supplying the rated load torque. Rated speed of this motor at rated torque is 1774.61 rpm. Fig. 2.6(a) and 2.6(b) shows that the q-axis currents do not go to zero at steady state, as was seen in the previous case and at rated torque stator currents has same magnitude. Fig. 2.7 shows that the phase currents will have higher rms value in this case than the no load values. This final rms value would be considered as the rated current of the motor. In Fig. 2.8, we see that the transients in torque, is having substantial value for a period greater than that in no load case. Then finally it settles to the value of rated load. Fig. 2.9 also shows that the motor takes longer time to settle to it's steady state operation. Fig. 2.10 shows the torque-speed characteristics for this period of free

acceleration with rated load torque.

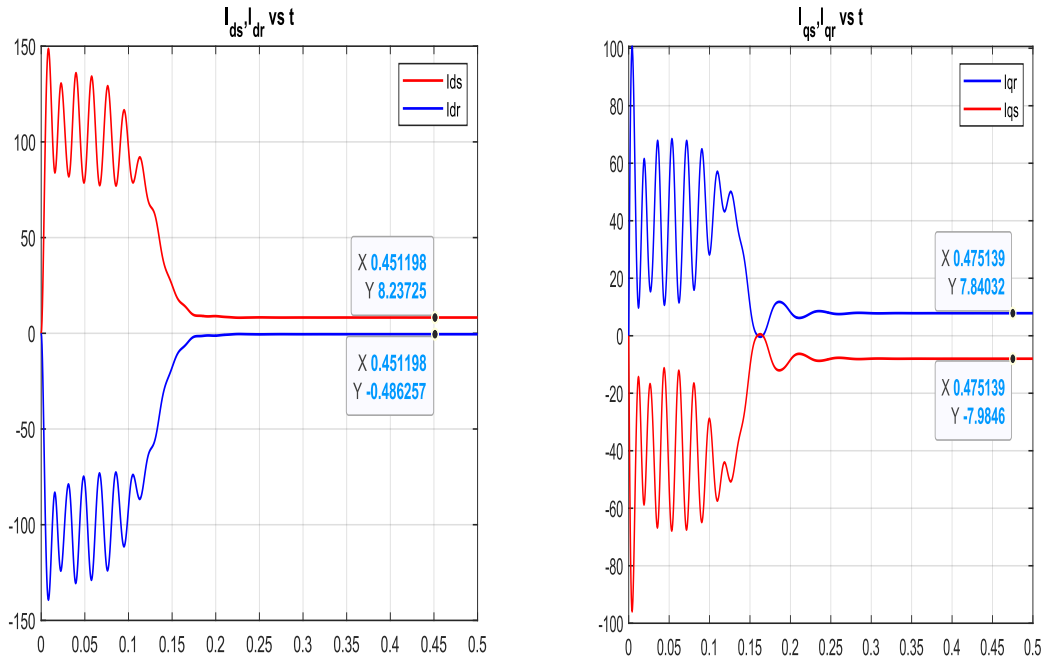

Figure 2.6(a) and 2.6(b) shows the d-axis and the q-axis currents of the motor at rated load

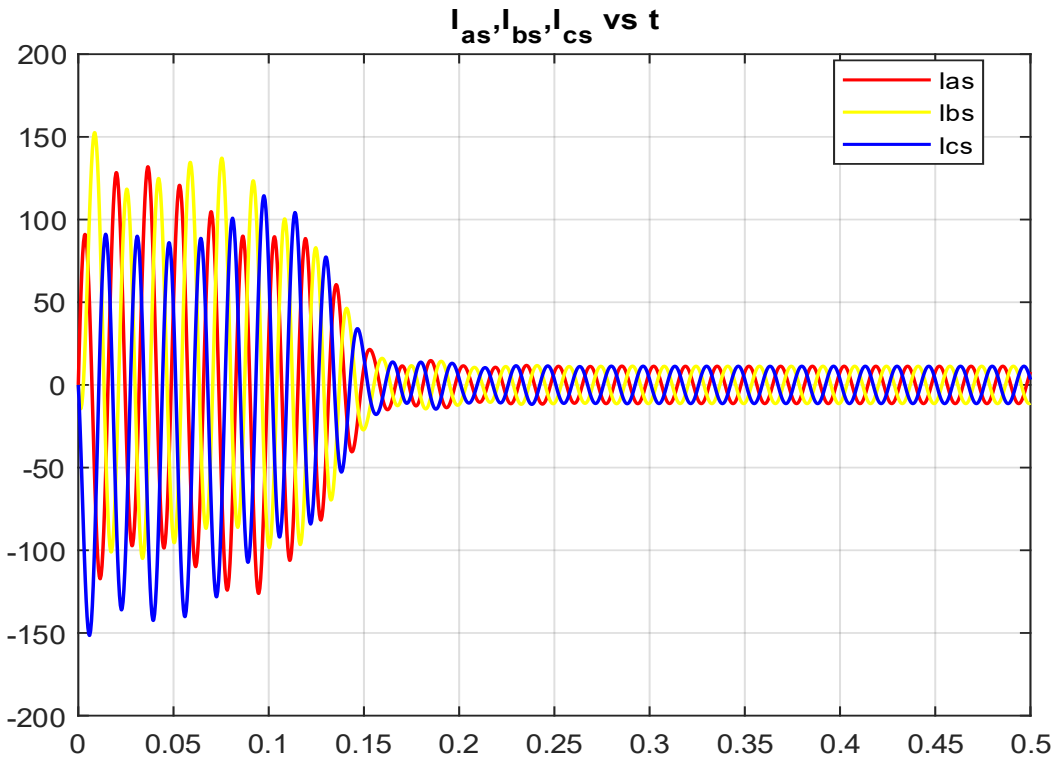

Figure 2.7 shows the three phase currents of the motor for free acceleration at Rated load

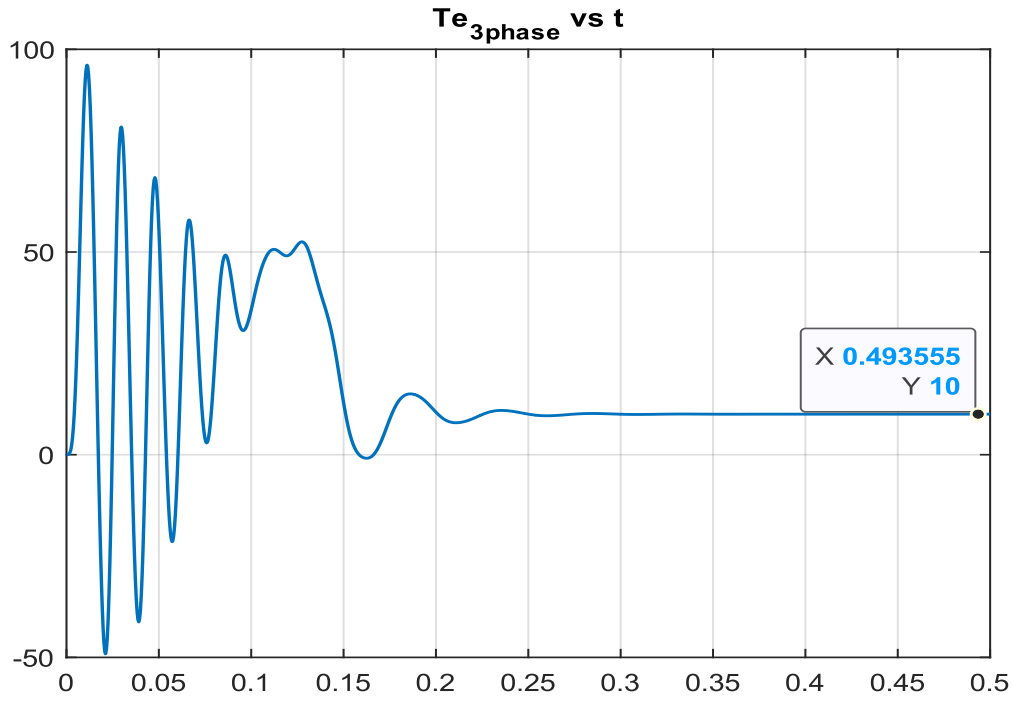

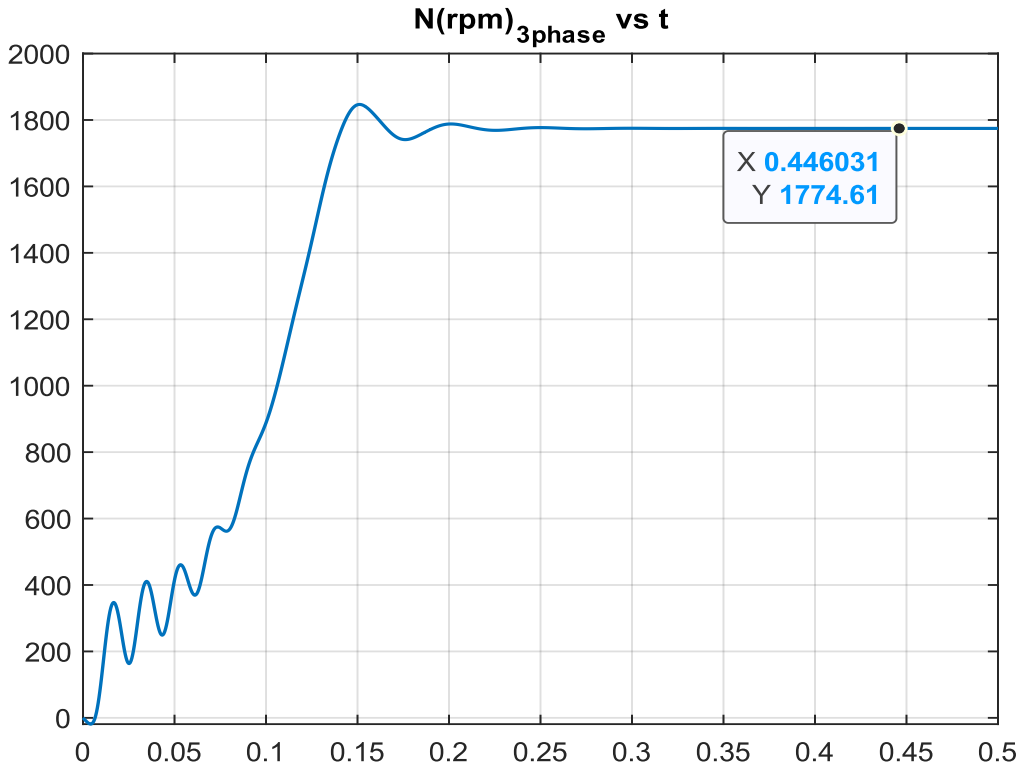

Figure 2.9 shows Speed (RPM) of the motor for free acceleration at rated load

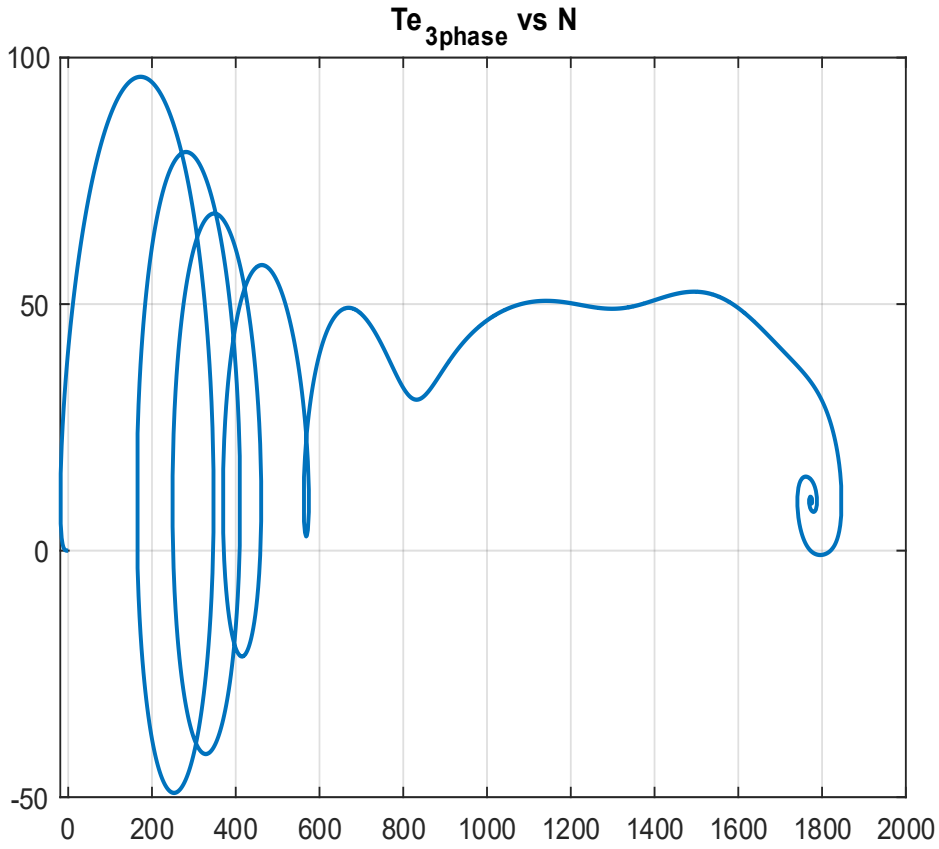

Figure 2.10 shows Torque vs Speed of the motor for free acceleration at rated load

Chapter 3

SPACE VECTOR PULSE WIDTH MODULATION

CHAPTER 3

SPACE VECTOR PULSE WIDTH MODULATION

3.1 Introduction of SVPWM

In recent years, Space Vector Pulse Width Modulation (SVPWM) has emerged as a widely adopted modulation technique for three-phase voltage source inverters (VSIs), particularly in the fields of renewable energy systems (RES) and alternating current (AC) motor drives. SVPWM offers several notable advantages over conventional Sinusoidal Pulse Width Modulation (SPWM), including lower harmonic distortion in the inverter output voltages and currents, improved utilization of the DC bus voltage, and reduced switching losses.

Initially, SVPWM was employed primarily for the analysis of AC machine operation. However, with suitable adaptations, it has been effectively utilized for the control of AC machines and inverters in RES applications. Although SVPWM involves more complex computations compared to SPWM, the advancement of digital control technology specifically modern microprocessors and digital signal processors has facilitated its practical implementation in real-time systems.

Traditional PWM techniques such as SPWM modulate each phase-leg of the inverter independently, resulting in three separate phase voltages. This approach is effective when the load's neutral point is connected to the inverter's grounded neutral, allowing each phase to operate independently. However, when the load is a three-phase machine with an isolated neutral point, the three phase-leg voltages become interdependent. In such cases, the current in one phase-leg is influenced by the voltages applied to the other two phases a dynamic that is not captured by SPWM.

Conversely, SVPWM inherently considers this interdependence by treating the inverter as a single entity. Rather than operating on individual phase voltages, SVPWM is based on line-to-line voltages and the synthesis of voltage space vectors. The technique employs the concept of space vectors, which represent the possible switching states of the inverter, and modulates the gating pulses of the semiconductor switches by comparing these space vectors with a desired reference vector. This approach enables more accurate voltage synthesis and dynamic performance in AC motor drive applications.

he Space Vector Pulse Width Modulation (SVPWM) technique uses a rotating voltage

space vector as the reference, replacing traditional three-phase modulating waveforms. When a sinusoidal signal is used as the reference, this voltage vector | $\overrightarrow{V_{ref}}$ |.maintains a constant magnitude | $\overrightarrow{V_{ref}}$ |.and rotates at a fixed frequency f_o , which corresponds to the fundamental frequency of the output voltage. The rotation occurs counterclockwise, following the standard a-b-c phase sequence. The amplitude of the resulting phase voltage is directly related to the magnitude of | $\overrightarrow{V_{ref}}$ |.

3.2 Switching states of a three phase two level inverter

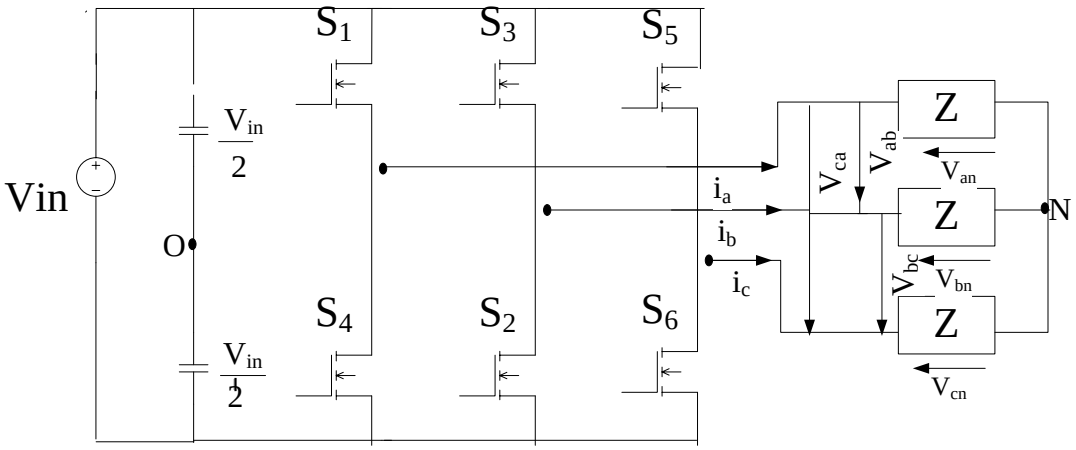

Figure 3.1 Conventional three-phase two-level voltage source inverter with balanced load

Fig 3.1 illustrates a typical three-phase voltage source inverter (VSI) topology used to supply a three-phase load. It uses six semiconductor switches (S_1 to S_6) arranged in three inverter legs corresponding to each output phase: a, b, and c. Each leg consists of a top switch (S_1, S_3, S_5) and a bottom switch (S_4, S_2, S_6). The inverter is powered by a split DC supply, where V_{in} is divided equally across two capacitors, providing a neutral point O. The switches operate with complementary gating signals, meaning that for each leg, when the top switch is ON (switching function = 1), the bottom switch is OFF (switching function = 0), and vice versa. The switching functions S_a, S_b, S_c and their complements $\bar{S}_a, \bar{S}_b, \bar{S}_c$ control which switches are conducting. These functions are binary in nature: 1 represents a conducting (ON) state and 0 a non-conducting (OFF) state. Because the switches are complementary in each leg, knowing the top switch states is sufficient to determine the inverter's behaviour. There are eight possible combinations for the top switches, forming $2^3 = 8$ distinct switching states. Among these, six are active states that generate line-to-line voltages and

contribute to motor torque, while the remaining two are zero states ([000] and [111]), which result in zero voltage at the output when the load is balanced.

Therefore, the output voltages of the inverter w.r.t the switching matrix $[S_a \ S_b \ S_c]^T$ can be generated using following equations:

$$\begin{bmatrix} v_{aN} \\ v_{bN} \\ v_{cN} \end{bmatrix} = \frac{V_{in}}{3} \begin{bmatrix} 2 & -1 & -1 \\ -1 & 2 & -1 \\ -1 & -1 & 2 \end{bmatrix} \begin{bmatrix} S_a \\ S_b \\ S_c \end{bmatrix} \tag{3.1}$$

$$\begin{bmatrix} v_{aN} \\ v_{bN} \\ v_{cN} \end{bmatrix} = V_{in} \begin{bmatrix} 1 & -1 & 0 \\ 0 & 1 & -1 \\ -1 & 0 & 1 \end{bmatrix} \begin{bmatrix} S_a \\ S_b \\ S_c \end{bmatrix} \tag{3.2}$$

Also, as it is for the balanced 3 phase supply

$$\begin{bmatrix} v_{aN} \\ v_{bN} \\ v_{cN} \end{bmatrix} = \frac{1}{3} \begin{bmatrix} 2 & -1 & -1 \\ -1 & 2 & -1 \\ -1 & -1 & 2 \end{bmatrix} \begin{bmatrix} v_{ao} \\ v_{bo} \\ v_{co} \end{bmatrix} \tag{3.3}$$

$$\begin{bmatrix} v_{aN} \\ v_{bN} \\ v_{cN} \end{bmatrix} = \frac{1}{3} \begin{bmatrix} 1 & 0 & -1 \\ -1 & 1 & 0 \\ 0 & -1 & 1 \end{bmatrix} \begin{bmatrix} v_{ab} \\ v_{bc} \\ v_{ca} \end{bmatrix} \tag{3.4}$$

And the corresponding line currents are influenced by the switching states, enabling **modulation of output voltages** through **pulse width modulation (PWM)** techniques.

Table 3.1 Switching Combinations and Normalized Output Voltages for a Three-Phase Two-Level Inverter

Inverter switching state	**Switching states of the semiconductor Switches**			**vaN**	**vbN**	**vcN**	**vab**	**vbc**	**vca**
	Sa	Sb	Sc						
1	0	0	0	0	0	0	0	0	0
2	0	0	1	-1/3	-1/3	2/3	0	-1	1
3	0	1	0	-1/3	2/3	-1/3	-1	1	0
4	0	1	1	-2/3	1/3	1/3	-1	0	1
5	1	0	0	2/3	-1/3	-1/3	1	0	-1
6	1	0	1	1/3	-2/3	1/3	1	-1	0
7	1	1	0	1/3	1/3	-2/3	0	1	-1
8	1	1	1	0	0	0	0	0	0

3.3 Clarke and Park Transformation

In power electronics systems, the Clarke and Park transformations are commonly used to simplify control circuits. Typically, voltages and currents in these systems are represented by three sinusoidal waveforms corresponding to the three AC phases (a, b, and c). Performing calculations directly in this a-b-c frame can be quite complex because of the continuously changing sinusoidal signals. However, when dealing with balanced three-phase systems, applying the Clarke and Park transformations converts these AC signals into two steady DC quantities, making the control process much simpler and more efficient.

$$\overrightarrow{V_s} = \frac{2}{3}\left[v_{aN} + v_{bN}e^{j\frac{2\pi}{3}} + v_{cN}e^{j\frac{4\pi}{3}}\right] \quad (3.5)$$

Where,

$\overrightarrow{V_s}$ is load phase voltage vector

v_{aN}, v_{bN}, v_{cN} is instantaneous values of the load phase voltages

Eq. (2.5) can be written as:

$$\overrightarrow{V_s} = \frac{2}{3}[v_{aN} + v_{bN}(cos120° + jsin120°) + v_{cN}(cos240° + jsin240°)] \quad (3.6)$$

$$\overrightarrow{V_s} = \frac{2}{3}\left[v_{aN} + v_{bN}\left(\frac{-1}{2} + j\frac{\sqrt{3}}{2}\right) + v_{cN}\left(\frac{-1}{2} + j\frac{\sqrt{3}}{2}\right)\right] \quad (3.7)$$

As $v_{aN} + v_{bN} + v_{cN} = 0$ for three phase balanced output voltage and load then Eq. (3.7)

Can be written as follows:

$$\overrightarrow{V_s} = v_{aN} + j\frac{1}{\sqrt{3}}(v_{bN} - v_{cn}) \quad (3.8)$$

$$\overrightarrow{V_s} = v_{\alpha} + jv_{\beta} \quad (3.9)$$

Where,

$$v_{\alpha} = v_{aN} \quad (3.10)$$

$$v_\beta = \frac{1}{\sqrt{3}}(v_{bN} - v_{cn}) \quad (3.11)$$

Eq.(2.10) and Eq(2.11) can be written in polar form as:

$$\overrightarrow{V_S} = |V_s| \angle \theta \quad (3.12)$$

Where,

$|V_s|$= amplitude of the sector $\overrightarrow{V_S} = \sqrt{(v_\alpha)^2 + (v_\beta)^2}$ (3.13)

θ = Phase angle of the vector $\overrightarrow{V_S} = tan^{-1}\left(\frac{v_\beta}{v_\alpha}\right)$ (3.14)

By using Eq. (3.10), Eq. (3.11), Eq. (3.13), Eq. (3.14) In a three-phase system, the time-varying or stationary voltages v_{aN}, v_{bN}, v_{cN} which are 120° out of phase with each other, can be converted into two-phase voltages v_a and v_b that are 90° apart. This conversion is known as the Clarke transformation. It plays a crucial role in generating reference signals for space vector PWM (Pulse Width Modulation) control techniques. For balanced three-phase systems, this transformation is expressed using the following equation:

$$\begin{bmatrix} v_\alpha \\ v_\beta \end{bmatrix} = \frac{2}{3}\begin{bmatrix} 1 & -\frac{1}{2} & -\frac{1}{2} \\ 0 & \frac{\sqrt{3}}{2} & -\frac{\sqrt{3}}{2} \\ \frac{1}{2} & \frac{1}{2} & \frac{1}{2} \end{bmatrix}\begin{bmatrix} v_{aN} \\ v_{bN} \\ v_{cN} \end{bmatrix} \quad (3.15)$$

The Clarke transformation for any variable f in a balanced three-phase system is typically used to convert three-phase quantities into a two-phase representation. This transformation simplifies the analysis and control of the system and is generally expressed as follows:

$$\begin{bmatrix} f_\alpha \\ f_\beta \end{bmatrix} = \frac{2}{3}\begin{bmatrix} 1 & -\frac{1}{2} & -\frac{1}{2} \\ 0 & \frac{\sqrt{3}}{2} & -\frac{\sqrt{3}}{2} \\ \frac{1}{2} & \frac{1}{2} & \frac{1}{2} \end{bmatrix}\begin{bmatrix} f_a \\ f_b \\ f_c \end{bmatrix} \quad (3.16)$$

And its inverse

$$\begin{bmatrix} f_a \\ f_b \\ f_c \end{bmatrix} = \begin{bmatrix} 1 & 0 & 1 \\ -\frac{1}{2} & \frac{\sqrt{3}}{2} & 1 \\ -\frac{1}{2} & -\frac{\sqrt{3}}{2} & 1 \end{bmatrix} \begin{bmatrix} f_\alpha \\ f_\beta \end{bmatrix} \quad (3.17)$$

When $f_a + f_b + f_c = 0$

Table 3.2 $\alpha\beta$ Frame Representation of Switching Vectors for a Three-Phase Two-Level Inverter

Load Phase voltage Vectors	Switching Vectors			Vα	Vß	Vα+vß	Θ
	Sa	Sb	Sc				
$\overrightarrow{V_0}$ Freewheeling	0	0	0	0	0	0	0°
$\overrightarrow{V_5}$ Active and Base	0	0	1	$-\frac{1}{3}$	$-\frac{1}{\sqrt{3}}$	$-\frac{1}{3}-j\frac{1}{\sqrt{3}}$	240°
$\overrightarrow{V_3}$ Active and Base	0	1	0	$-\frac{1}{3}$	$\frac{1}{\sqrt{3}}$	$-\frac{1}{3}+j\frac{1}{\sqrt{3}}$	120°
$\overrightarrow{V_4}$ Active	0	1	1	$-\frac{2}{3}$	0	$-\frac{2}{3}$	-180°
$\overrightarrow{V_1}$ Active and base	1	0	0	$\frac{2}{3}$	0	1	0°
$\overrightarrow{V_6}$ Active	1	0	1	$\frac{1}{3}$	$-\frac{1}{\sqrt{3}}$	$\frac{1}{3}-j\frac{1}{\sqrt{3}}$	-60°
$\overrightarrow{V_2}$ Active	1	1	0	$\frac{1}{3}$	$\frac{1}{\sqrt{3}}$	$\frac{1}{3}+j\frac{1}{\sqrt{3}}$	60°
$\overrightarrow{V_7}$ Freewheeling	1	1	1	0	0	0	0°

By Eq (3.10) to (3.17) and Table 3.1, Table 3.2 lists the eight possible switching vectors along with the corresponding normalized load phase voltage vectors, represented in the complex plane as $v_\alpha + jv_\beta$.

The space voltage vectors $\overrightarrow{V_1}$, $\overrightarrow{V_2}$, $\overrightarrow{V_3}$, $\overrightarrow{V_4}$, $\overrightarrow{V_5}$ and $\overrightarrow{V_6}$ form a hexagonal shape, dividing the plane into six equal sectors of 60° each. The six switching states [100], [110], [010], [011], [001], and [101] are referred to as active states, while the remaining two states [000] and

[111] are known as zero or freewheeling states. Once the basic switching states [100], [010], and [001] are known, the other states can be derived from them.

From this point forward, the space vector representation of the three-phase, two-level inverter's switching states will be used for implementing the Space Vector Pulse Width Modulation (SVPWM) technique.

In addition to the Clarke transformation, another important mathematical tool used in control systems is the Park transformation. This transformation converts three-phase quantities (a-b-c frame) or two-phase orthogonal components (α-β frame) into a rotating reference frame known as the d-q (direct-quadrature) frame. The result is a set of time-invariant DC quantities rather than time-varying AC waveforms. This simplification enables the effective use of standard control strategies such as Proportional-Integral-Derivative (PID) controllers, thereby streamlining the control system design. The Park transformation for any three-phase variable f is defined by the following equations:

$$\begin{bmatrix} f_q \\ f_d \\ f_0 \end{bmatrix} = \frac{2}{3}\begin{bmatrix} cos(\omega_e t) & cos(\omega_e t - 120^o) & cos(\omega_e t - 240^o) \\ sin(\omega_e t) & sin(\omega_e t - 120^o) & sin(\omega_e t - 240^o) \\ \frac{1}{2} & \frac{1}{2} & \frac{1}{2} \end{bmatrix}\begin{bmatrix} f_a \\ f_b \\ f_c \end{bmatrix} \tag{3.18}$$

Here, f_0 represents the zero-sequence component, and ω_e is the angular speed of the rotating reference frame. For a balanced three-phase system, the Park transformation simplifies to the following form:

And its inverse

$$\begin{bmatrix} f_a \\ f_b \\ f_c \end{bmatrix} = \begin{bmatrix} cos(\omega_e t) & sin(\omega_e t) & 1 \\ cos(\omega_e t - 120^o) & sin(\omega_e t - 120^o) & 1 \\ cos(\omega_e t - 240^o) & sin(\omega_e t - 240^o) & 1 \end{bmatrix}\begin{bmatrix} f_q \\ f_d \\ f_0 \end{bmatrix} \tag{3.19}$$

Furthermore, for a balanced three-phase system, the Park transformation that converts variables from the α-β (stationary) reference frame to the d-q (rotating) reference frame is expressed as follows:

$$\begin{bmatrix} f_d \\ f_q \end{bmatrix} = \begin{bmatrix} cos(\omega_e t) & sin(\omega_e t) \\ -sin(\omega_e t) & cos(\omega_e t) \end{bmatrix}\begin{bmatrix} f_\alpha \\ f_\beta \end{bmatrix} \text{ when } f_a + f_b + f_c = 0 \tag{3.20}$$

And its inverse

$$\begin{bmatrix} f_\alpha \\ f_\beta \end{bmatrix} = \begin{bmatrix} cos(\omega_e t) & sin(\omega_e t) \\ -sin(\omega_e t) & cos(\omega_e t) \end{bmatrix} \begin{bmatrix} f_d \\ f_q \end{bmatrix} \quad (3.21)$$

3.4 Steps for Implementing SVPWM Technique 3Φ Two-Level VSI

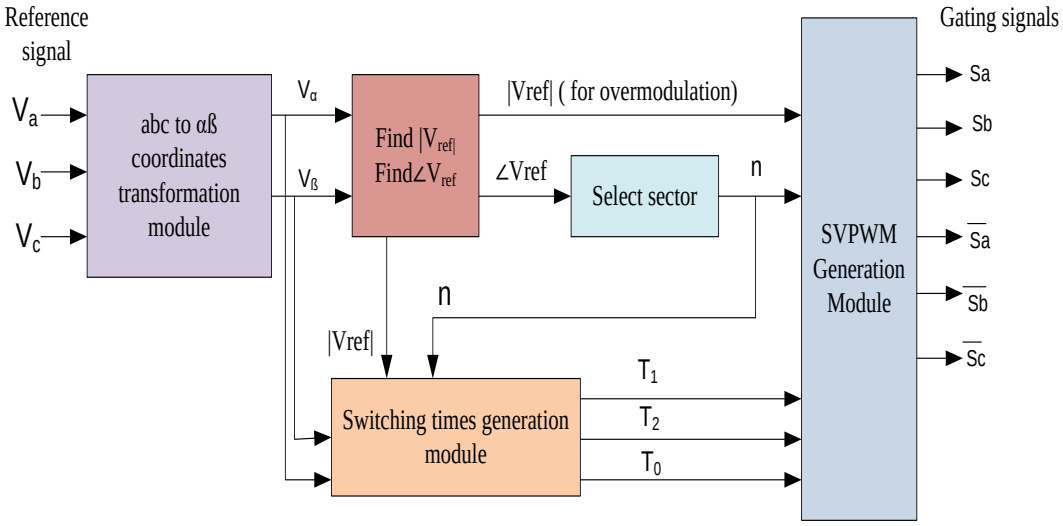

Figure 3.2: Schematic diagram of SVPWM

To implement the SVPWM (Space Vector Pulse Width Modulation) technique, the following steps are followed:

Step 1:

Begin by reading the three-phase AC reference voltages, (v_a, v_b, v_c) just as done in the SPWM method.

Step 2:

Convert these three-phase voltages into two-phase components in the α-β (stationary) reference frame using the Clarke transformation. In other words: (va,vb,vc)→(vα,vβ)

Step 3:

Determine the magnitude of the vα and vβ components, and calculate the phase angle of the resulting reference vector using the appropriate mathematical expressions.

$$|\overrightarrow{V_{ref}}| = \sqrt{(v_\alpha)^2 + (v_\beta)^2} \text{ and } \theta = \angle\overrightarrow{V_{ref}} = tan^{-1}\left(\frac{v_\beta}{v_\alpha}\right) = \omega t = 2\pi f_o t$$

$$f_o = frequency\ of\ output\ fundamental\ voltage$$

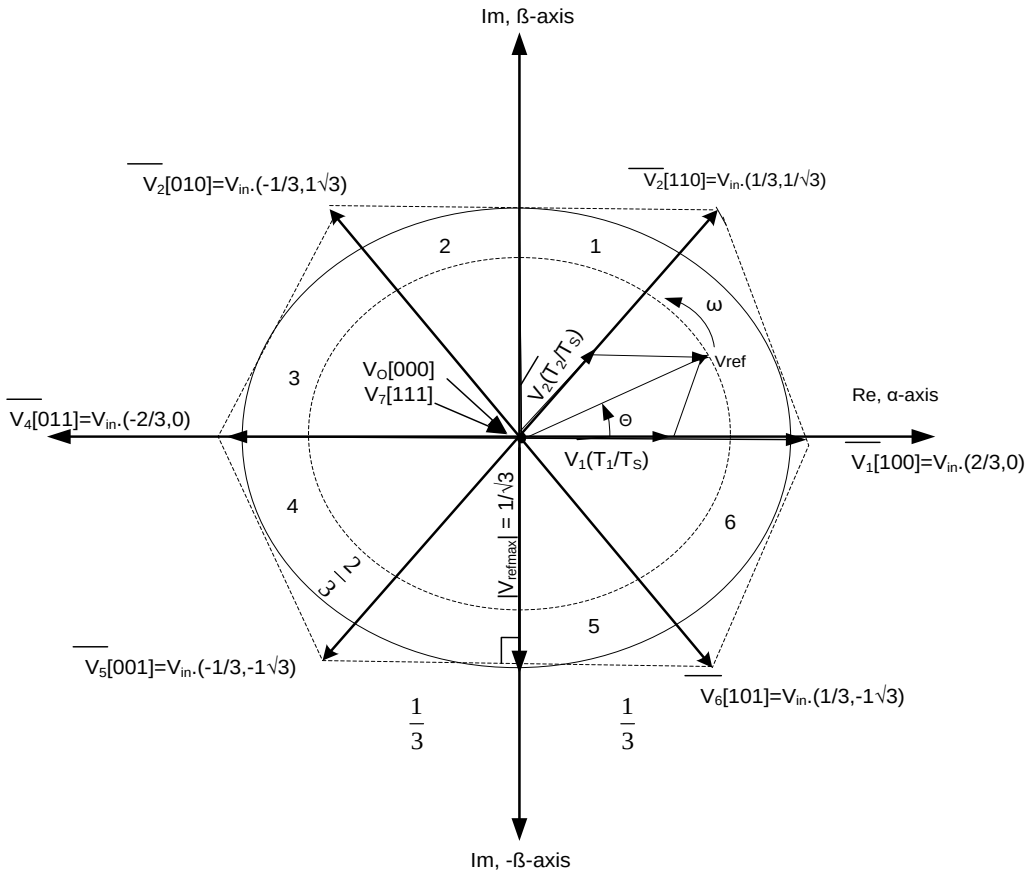

Figure 3.3 Vector diagram of SVPWM

Step 4:

An arbitrary reference output voltage vector is created $\overrightarrow{V_{ref}}$ by geometric summation of $\overrightarrow{V_1}$ + $\overrightarrow{V_2}$ which are the two nearest space vectors.

Each sector of the space vector diagram is divided into N equal switching intervals. The duration of each interval is given by:

$T_s = \frac{T_o}{N}$ where T_o is the period of the output voltage.

When the reference voltage signal is sinusoidal, the frequency of the inverter's output matches the rotational speed of the reference vector $\overrightarrow{V_{ref}}$ .Meanwhile, the output voltage magnitude is determined by the length (or magnitude) of $\overrightarrow{V_{ref}}$. The reference vector $\overrightarrow{V_{ref}}$. completes one full rotation for every cycle of the inverter's fundamental output frequency. By using a high switching frequency typically 100 to 1000 times higher than the fundamental frequency the reference vector can be considered nearly constant during a single switching interval T_s.

As illustrated in Fig. (3.3), the maximum output voltage achievable with the SVPWM technique corresponds to the radius of the largest circle that can be inscribed within the hexagon formed by the active space vectors. This circle touches the midpoints of the sides of the hexagon and represents the highest fundamental voltage amplitude that can be generated without distortion. This circle touches the midpoints of the lines connecting the tips of the active space vectors. As illustrated in Fig. (3.3), the maximum amplitude of the fundamental output voltage that can be achieved using the SVPWM technique is: $\left|\overrightarrow{V_{ref}}\right|_{max} = V_{in}/\sqrt{3} = 0.5774V_{in}$. In comparison, the maximum output voltage attainable using traditional SPWM is: $\left|\overrightarrow{V_{ref}}\right|_{max} = 0.5V_{in}$. Therefore, SVPWM allows for an increase of approximately 15.4% in the output voltage, making it more efficient in utilizing the available DC bus voltage.

Step 5:

Determine the sector in which the reference voltage vector $\overrightarrow{V_{ref}}$ is located.

Fig. (3.4) shows a step-by-step algorithm for identifying the sector based on the known values of the v_α and v_β components.

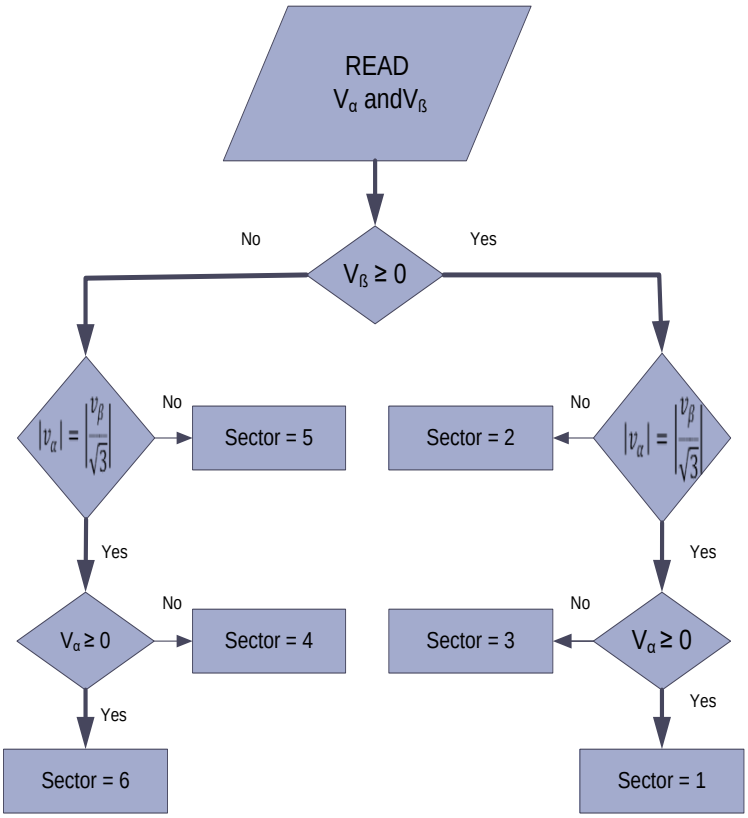

Figure 3.4 Algorithm of sector determination

Step 6: Choose the appropriate stationary (non-rotating) switching vectors that belong to the sector in which the reference voltage vector $\overrightarrow{V_{ref}}$ has been identified. These vectors will be used to synthesize the desired output during that switching interval.

Step7: Calculation of Dwell Times T_1, T_2 *and* T_0

After determining the sector and selecting the corresponding switching vectors, the next step is to calculate the duration for which each vector should be applied within a switching cycle. These time intervals—known as dwell times T_1, T_2 *and* T_0 are computed based on the magnitude of the reference voltage vector $\overrightarrow{V_{ref}}$ and its phase angle θ. Accurate calculation of these times ensures the reference vector is correctly synthesized, producing the desired output voltage.

An arbitrary reference output voltage vector $\overrightarrow{V_{ref}}$ is generated by combining multiple space vectors within a single switching cycle T_s, as illustrated in Fig. (3.3). During each switching period, this combination is achieved through geometric summation, which can be described mathematically as follows:

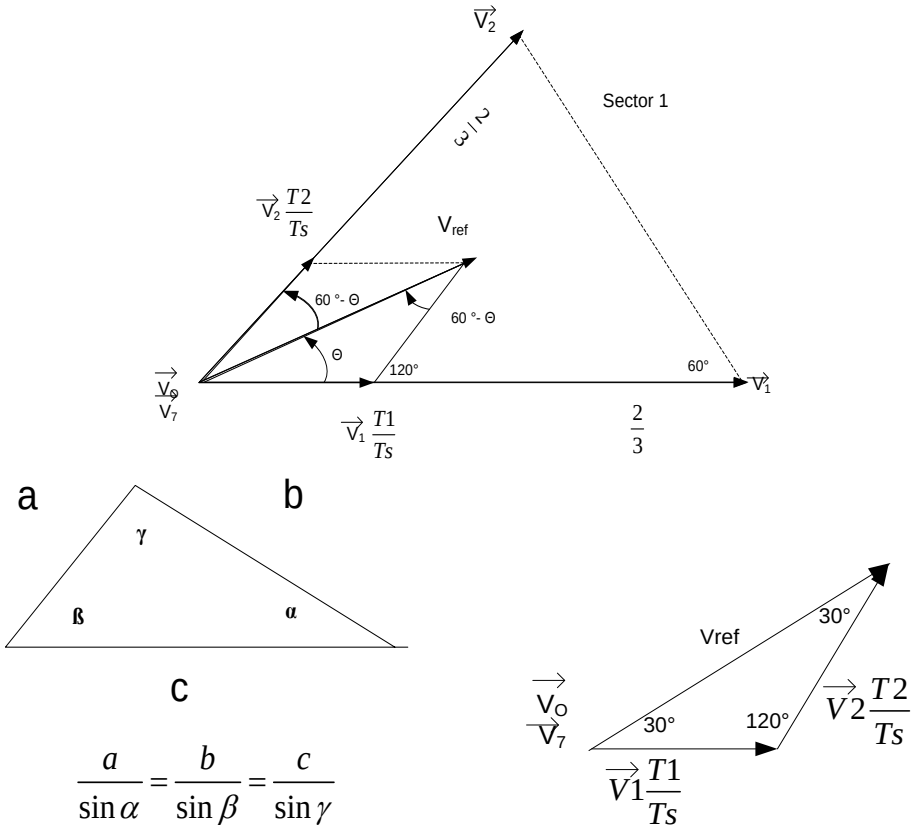

$$\frac{a}{\sin\alpha} = \frac{b}{\sin\beta} = \frac{c}{\sin\gamma}$$

Figure 3.5 Sector 1 calculation diagram

$$\vec{V}_{ref}T_s = (v_\alpha + \mathrm{j}v_\beta)T_s = |V_{ref}|(cos(\theta) + j\,sin(\theta))\,T_s = \vec{V}_1T_1 + \vec{V}_2T_2 \qquad (3.22)$$

$$\frac{|\vec{V}_1|T_1}{sin(60^o-\theta)} = \frac{|\vec{V}_{ref}|T_s}{sin(120^o)} \text{ and } \frac{|\vec{V}_2|T_1}{sin(\theta)} = \frac{|\vec{V}_{ref}|T_s}{sin(120^o)} \qquad (3.23)$$

From Fig. (3.5), the equations can be:

$$\left|\overrightarrow{V_1}\right| = \left|\overrightarrow{V_2}\right| = \frac{2}{3}V_{in} \qquad (3.24)$$

$$T_1 = \frac{\frac{2}{\sqrt{3}}|\vec{V}_{ref}|\,sin(60^o-\theta)}{\frac{2}{3}V_{in}}T_s = T_s m_a\,sin(60^o-\theta) \qquad (3.25)$$

$$T_2 = \frac{\frac{2}{\sqrt{3}}|\vec{V}_{ref}|\,sin(\theta)}{\frac{2}{3}V_{in}}T_s = T_s m_a \sin\theta \qquad (3.26)$$

Where $m_a = \frac{\sqrt{3}|\vec{V}_{ref}|}{V_{in}}$ =amplitude of modulation factor

The zero vectors are applied during the remaining time of the switching cycle that is not occupied by the active vectors. Therefore, the total duration for which the zero vectors are used within one switching period is calculated as:

$$T_0 = T_s - T_1 - T_2 \qquad (3.27)$$

Eq. (2.25) and Eq. (2.26) are only applicable for Sector 1. The generalise equations for $T_1\ and\ T_2$ is

$$T_1 = T_s m_a\,sin\left(60^o - \theta - \frac{n-1}{3}\pi\right)$$

$$T_2 = T_s m_a\,sin\left(\theta - \frac{n-1}{3}\pi\right) \qquad (3.28)$$

Where n=sector number =1,2,3,4,5,6

Step 8: Determine the switching vector sequence using a symmetrical scheme

The sequence in which the switching vectors are applied depends on the chosen SVPWM strategy. The selection of the zero vector whether using only V_0 *and* V_7, or alternating between both defines the specific modulation approach.

One commonly used method is the symmetric 7-segment technique. In this approach, the zero vectors are alternated in each switching cycle, and the sequence of active vectors is reversed after each zero vector. This symmetrical pattern helps minimize harmonic distortion and improves the quality of the output waveform.

In the symmetrical 7-segment SVPWM method, the sequence $\overrightarrow{V_0} \rightarrow \overrightarrow{V_1} \rightarrow \overrightarrow{V_2} \rightarrow \overrightarrow{V_7}$ is applied during the first half of the switching period $T_s/2$, and the reverse sequence $\overrightarrow{V_7} \rightarrow \overrightarrow{V_2} \rightarrow \overrightarrow{V_1} \rightarrow \overrightarrow{V_0}$ is applied in the second half.

These sequences are symmetrical, and the switching frequency matches the inverter's sampling frequency. To maintain a fixed switching frequency and achieve optimal harmonic performance, each phase leg of the inverter should switch only once per switching cycle. This is accomplished by placing the zero vector at the beginning and end of the sequence and applying the two adjacent active vectors in between, all within a half switching period.

Step 9: Apply gating signals to each phase-leg of the inverter

Once the dwell times $T_1, T_2,$ and T_0 are calculated (as shown in Table 2.3), the corresponding duty cycles for the inverter switches can be determined. These duty cycles define how long each switch remains on during a switching period.

For instance, if the reference voltage vector $\overrightarrow{V_{ref}}$ lies in sector 1, the duty cycles for the switches in each phase leg can be derived based on the calculated vector durations. These duty cycles are then used to generate the gating signals that control the on/off states of the inverter switches.

$$ds_1 = \frac{T_1+T_2+\frac{T_0}{2}}{\frac{T_s}{2}} \qquad ds_3 = \frac{T_2+\frac{T_0}{2}}{\frac{T_s}{2}} \qquad ds_5 = \frac{\frac{T_0}{2}}{\frac{T_s}{2}} \tag{3.29}$$

$$ds_4 = \frac{T_0}{\frac{T_s}{2}} \qquad ds_6 = \frac{T_1+\frac{T_0}{2}}{\frac{T_s}{2}} \qquad ds_2 = \frac{T_1+T_2+\frac{T_0}{2}}{\frac{T_s}{2}} \tag{3.30}$$

Step 10: Output voltage is generated at the output of the inverter.

Table3.3 Dwell Time of Switching and Every Sector

Sector	Duration times of upper switches S_1,S_3,S_5	Duration times of lower switches S_4,S_6,S_2
1	Sa = T1+ T2+ To/2 Sb = T2+To/2 Sc = To/2	Sa = To/2 Sb = T1+To/2 Sc = T1+ T2 +To/2
2	Sa= T1+T0=2 Sb = T1 +T2+To/2 Sc = To/2	Sa = T2+To/2 Sb = To/2 Sc = T1+ T2+ To/2
3	Sa = To/2 Sb = T1+T2+To/2 Sc = T2+ To/2	Sa = T1+T2+To/2 Sb = To/2 Sc = T1+ To/2
4	Sa = To/2 Sb = T1+To/2 Sc = T1+ T2 +To/2	Sa = T1+ T2+ To/2 Sb = T2+To/2 Sc = To/2
5	Sa = T2+To/2 Sb = To/2 Sc = T1+ T2+ To/2	Sa= T1+T0=2 Sb = T1 +T2+To/2 Sc = T0/2
6	Sa = T1+T2+To/2 Sb = To/2 Sc = T1+ To/2	Sa = To/2 Sb = T1+T2+To/2 Sc = T2+ To/2

3.6 Conclusion:

Simulink and code have been done of Clarke and Park Transformation whose results can be seen in further chapters and SVPWM technique is used for FOC which can also be seen in further chapters.

Chapter 4

CONTROL SCHEME FOR INDUCTION MOTOR DRIVES

CHAPTER 4

CONTROL SCHEME FOR INDUCTION MOTOR DRIVES

4.1 Introduction

Induction motor drives have long been the backbone of industrial variable speed applications, serving a wide power range from small fractional horsepower systems to large multi-megawatt installations. They are commonly used in a variety of sectors, including pumps and fans, paper and textile manufacturing, electric trains and subways, electric and hybrid vehicles, machine tools, robotics, and wind energy systems.

This chapter focuses on the control strategies used for operating induction motors in variable speed applications. Various control methods are available, such as scalar control, vector (or field-oriented) control, direct torque and flux control, and adaptive control. While scalar control is briefly discussed, the primary focus of this chapter is on vector control due to its superior performance and precision in dynamic applications.

4.2 Scalar Control of Induction Machine

Scalar control, as the name suggests, relies solely on adjusting the magnitude of control variables without considering the machine's coupling effects. For instance, voltage regulation can influence flux, while frequency or slip adjustments help manage torque. However, both flux and torque inherently depend on frequency and voltage variations. In scalar control, both the magnitude and phase alignment of vector variables are regulated. While scalar-controlled drives may not offer performance as refined as other control methods, they are relatively simple to implement. The following sections explore various scalar control techniques used with voltage-fed inverters.

4.2.1 Open Loop Volts/Hz Control

The open-loop Volts-per-Hertz (V/Hz) control strategy remains one of the most widely adopted methods for controlling the speed of induction motors, primarily due to its simplicity and reliability. Induction motors are extensively used across various industrial applications, often operating at constant speed with a standard 60 Hz power supply. However, in scenarios requiring variable speed operation, frequency control becomes

essential. To maintain a constant stator flux—critical for stable motor performance—the applied voltage must be adjusted in direct proportion to the frequency. This relationship holds under the assumption that stator resistance is negligible, allowing the flux linkage to remain steady as defined by the ratio $\psi_s = \frac{V_s}{\omega_s}$. Figure 4.1 illustrates the block diagram of the open-loop Volts-per-Hertz (V/f) control method. The power circuit includes a diode rectifier connected to either a single-phase or three-phase AC supply, followed by a filter and a PWM voltage-source inverter. This control strategy is straightforward and generally does not require any feedback signals.

In this method, the stator electrical frequency ω_e is the main control variable, as it directly influences the rotor speed ω_r. Since the slip speed is typically very small, ω_e can be considered approximately equal to ω_r under ideal conditions.

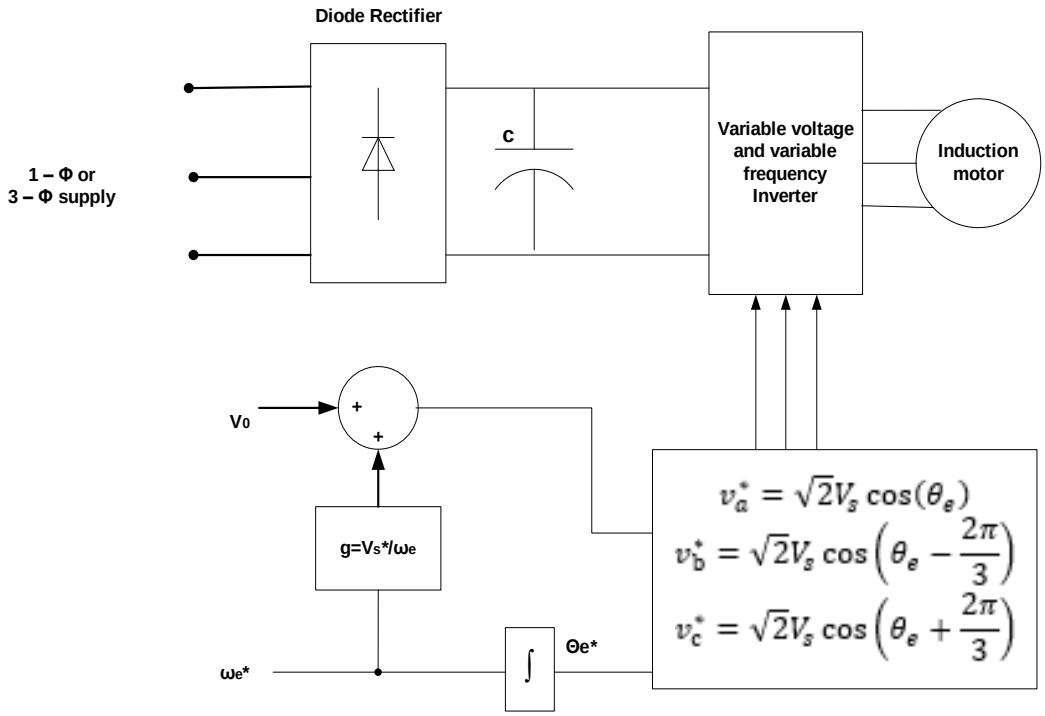

Figure 4.1: Block diagram of the open loop Volts/Hz control for an induction motor

The phase voltage V_s^* command is generated directly from the frequency command using a gain factor 'g', as illustrated in the control scheme. This relationship helps maintain a constant stator flux ψ_s. When the stator resistance and leakage inductance are considered negligible, this stator flux can be assumed to be nearly equal to the air-gap flux ψ_m or the rotor flux ψ_r.

However, at low operating speeds—where the stator frequency ω_e is also low the stator resistance consumes a significant portion of the applied voltage. This leads to a drop in the effective flux, which can weaken the motor's performance. To counter this effect, a boost voltage V_o is added to the phase voltage command. This additional voltage compensates for the voltage drop across the stator resistance, helping to maintain the rated flux and ensuring that the motor can still produce full torque down to zero speed.

The effect of V_o at higher frequencies is small. The ω_e^* signal is integrated to generate the angle θ_e^*

And the corresponding sinusoidal phase voltages (v_a^*, v_b^*, v_c^*) signals are generated as:

$$v_a^* = \sqrt{2}V_s \cos(\theta_e) \quad (4.1)$$

$$v_b^* = \sqrt{2}V_s \cos\left(\theta_e - \frac{2\pi}{3}\right) \quad (4.2)$$

$$v_c^* = \sqrt{2}V_s \cos\left(\theta_e + \frac{2\pi}{3}\right) \quad (4.3)$$

In this drive system, the PWM converter is integrated with the inverter stage. However, several challenges are associated with operating this open-loop control configuration:

Precise speed control of the induction motor is not achievable because the rotor speed ω_r is always slightly less than the synchronous speed ω_s. Since the stator frequency f_s, or equivalently the synchronous speed ω_s, is the only controllable variable in this setup, the actual rotor speed cannot be directly regulated.

The slip speed$\omega_{sl} = \omega_s - \omega_r$, which represents the difference between the synchronous speed and the rotor speed, cannot be maintained accurately. This is due to the absence of rotor speed feedback in this scheme. As a result, the motor may operate in the unstable region of its torque-speed characteristic curve, especially under varying load conditions.

These inaccuracies can cause the stator current to rise significantly above its rated value, which poses a risk to both the inverter and the converter components due to thermal and electrical stress.

To address these limitations, an outer speed control loop is introduced. In this improved scheme, the actual rotor speed ω_r is measured and compared with the reference speed ω_r^*.

The resulting error is processed through a controller typically a Proportional-Integral (PI) controller—and the output is passed through a limiter to generate the desired slip speed command ω_{sl}^{*}. This closed-loop arrangement enhances stability and improves speed regulation performance.

4.3 Vector Control of Induction Motor

Scalar control of induction motors is relatively straightforward to implement. However, it suffers from a key drawback flux and torque are both functions of voltage (or current) and frequency, which leads to strong coupling between the variables. This coupling results in a slow dynamic response and can even cause instability, especially since the system behaves like a high-order system.

When the torque demand is increased by raising the slip or the supply frequency fs, the magnetic flux ψ in the motor tends to decrease. Since the flux does not respond instantaneously, there is a delay before the flux control loop typically characterized by a large time constant can compensate for this drop. This momentary dip in flux reduces the sensitivity of torque to changes in slip 's', thereby prolonging the system's response time.

In scalar control, adjustments to the motor's behavior rely solely on changing the magnitude and frequency of the stator or rotor phase currents, but not their instantaneous phase angles. This means that variations in flux linkages ψ_s and ψ_r must be indirectly controlled, making the process less efficient.

By contrast, separately excited DC motor drives offer much simpler control because the flux ψ_f and torque Te can be regulated independently. This separation is achieved through independent control of the field current if and armature current ia. When the field flux is held constant, torque becomes directly controllable through the armature current alone. Additionally, DC drives only require control over current magnitudes, without the need for frequency or phase angle regulation—an advantage not shared by AC machines.

In the case of induction motor drives, such decoupled control is more complex. It requires coordinated regulation of the stator current's magnitude |is|, frequency fs, and phase angle θ. However, just like in DC drives, independent control of flux ψ and torque Te is achievable in AC drives using vector control techniques.

To do this, the stator current phasor $\vec{\imath_s}$ is decomposed into two orthogonal components one

aligned with the rotor flux linkage $\overrightarrow{\psi_r}$, which produces the magnetic field (flux-producing current), and the other perpendicular to it, which contributes to torque. For this decoupling to be effective, the instantaneous position of the rotor flux vector must be known.

With knowledge of this flux position, the control of an induction machine can closely mimic that of a DC motor. Modern inverter technology makes it possible to precisely regulate the stator current's phase, frequency, and magnitude, thereby enabling control in the rotor flux reference frame. This strategy is known as field-oriented control (FOC) or vector control, as it is based on phasor-level regulation of flux linkages rather than scalar values.

4.3.1 Principle of Vector Control

Vector control of an induction motor is typically described under the assumption that the position of the rotor flux linkage phasor λ_r is known. The corresponding phasor representation is illustrated in Figure 4.2. In this diagram, λ_r is positioned at an angle θ_f relative to the stationary reference frame. This angle θ_f is commonly referred to as the field angle.

To implement vector control, the three-phase stator currents are mathematically converted into two components direct-axis (d-axis) and quadrature-axis (q-axis) currents within a rotating reference frame that aligns with the rotor flux. This transformation is achieved through a mathematical coordinate transformation into the synchronous reference frame.

$$\begin{bmatrix} i_{qs} \\ i_{ds} \end{bmatrix} = \frac{2}{3} \begin{bmatrix} \cos\theta_f & \cos\left(\theta_f - \frac{2\pi}{3}\right) & \cos\left(\theta_f + \frac{2\pi}{3}\right) \\ \sin\theta_f & \sin\left(\theta_f - \frac{2\pi}{3}\right) & \sin\left(\theta_f + \frac{2\pi}{3}\right) \\ \frac{1}{2} & \frac{1}{2} & \frac{1}{2} \end{bmatrix} \begin{bmatrix} f_a \\ f_b \\ f_c \end{bmatrix} \tag{4.4}$$

From which the stator current phasor i_s is derived as:

$$|i_s| = \sqrt{\left(i_{qs}\right)^2 + (i_{ds})^2} \tag{4.5}$$

$$\theta = tan^{-1}\left(\frac{i_{qs}}{i_{ds}}\right) \tag{4.6}$$

where i_{qs} and i_{ds} are the 'q' and the 'd' axes currents in the synchronous reference frame that are obtained by projecting the stator current phasor on the 'q' and 'd' axes respectively.

The current phasor magnitude remains the same regardless of the reference frame chosen as is clear from Figure 4.2.

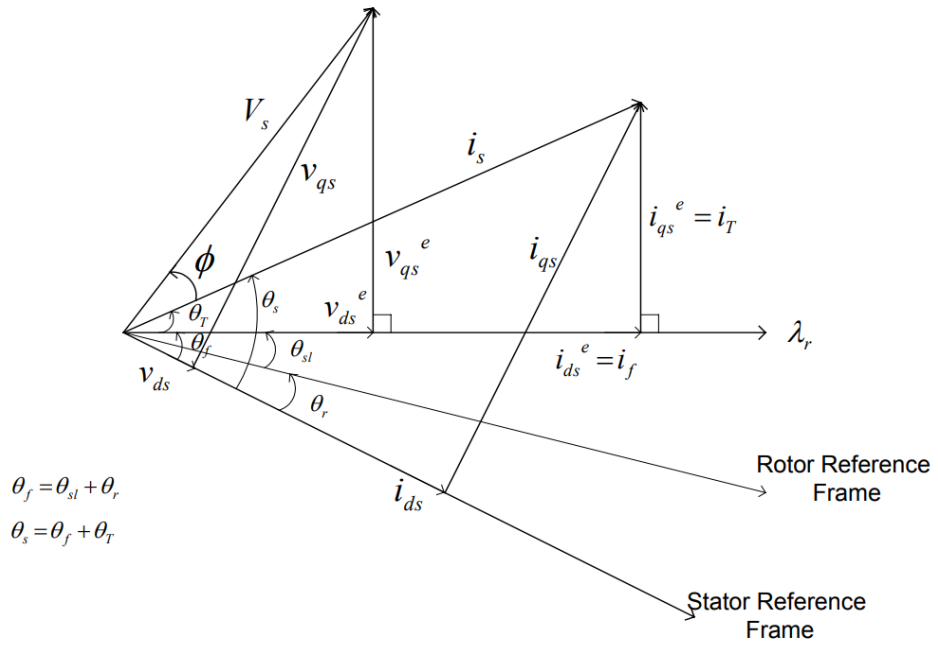

Figure 4.2: Phasor Diagram of Vector Controller

The stator current is responsible for generating both the rotor flux λ_r and the electromagnetic torque *Te*. To effectively produce the rotor flux, the component of the stator current contributing to it must be aligned in phase with λ_r . When the stator current phasor is broken down or resolved along the direction of λ_r , the resulting in-phase component is identified as the flux-producing component, as illustrated in Figure 4.2. Meanwhile, the component that lies perpendicular to λ_r is responsible for producing torque. Thus,

$$\lambda_r \propto i_f \tag{4.7}$$

$$T_e \propto \lambda_r i_T \propto i_f i_T \tag{4.8}$$

In steady-state conditions, the current components i_f *and* i_T remain as DC quantities because there is no relative motion between the synchronous reference frame and the rotor flux λ_r. Aligning the control with λ_r effectively places the analysis in a synchronous reference frame, where the flux-producing and torque-producing current components

appear as constant (DC) values. This characteristic makes them ideal for use as control variables. So far, it has been assumed that the position of the rotor flux is known. However, in practice, this field angle must be continuously calculated in real time. This angle, often referred to as the field angle, can be expressed as

$$\theta_f = \theta_{sl} + \theta_r \quad (4.9)$$

where θ_r is the rotor position and θ_{sl} is the slip angle. In terms of the speeds and time, the field angle can be written as

$$\theta_f = \int (\omega_r + \omega_{sl})\, dt = \int \omega_s\, dt \quad (4.10)$$

Vector control methods are categorized based on how the real-time position of the rotor flux is determined. These fall into two main types: direct vector control and indirect vector control.

In direct vector control, the field angle representing the rotor flux position is obtained using measurable quantities such as terminal voltages, stator currents, Hall-effect sensors, or specially designed flux-sensing windings. On the other hand, indirect vector control calculates the rotor flux position without directly measuring voltages or currents. Instead, it relies on known machine parameters and rotor position feedback, combining estimation techniques with position measurements to determine the field angle.

4.3.2 Derivation of Indirect Vector Control for Induction Motor

In the derivation for the indirect vector control scheme a current source inverter is assumed, in which case the stator phase currents serve as inputs, hence the stator dynamics can be neglected. The dynamic equations of the induction motor in the synchronous reference frame for the rotor taking flux as state variable is given as,

$$r_r i_{qr} + p\lambda_{qr} + \omega_{sl}\lambda_{dr} = 0 \quad (4.11)$$

$$r_r i_{dr} + p\lambda_{dr} - \omega_{sl}\lambda_{qr} = 0 \quad (4.12)$$

Where,

$$\omega_{sl} = \omega_s - \omega_r \quad (4.13)$$

$$\lambda_{qr} = L_r i_{qr} + L_m i_{qs} \quad (4.14)$$

$$\lambda_{dr} = L_r i_{dr} + L_m i_{ds} \quad (4.15)$$

The resultant rotor flux linkage, λr also known as the rotor flux linkages phasor is assumed to be on the direct axis to achieve field orientation. This alignment reduces the number of variables to deal. The alignment of the d-axis with rotor flux phasor yield

$$\lambda_r = \lambda_{dr} \tag{4.16}$$

$$\lambda_{qr} = 0 \tag{4.17}$$

$$p\lambda_{qr} = 0 \tag{4.18}$$

Substituting Equations 4.15 to 4.17 in Equations 4.11 and 4.12 causes the new rotor equations to be,

$$r_r i_{qr} + \omega_{sl}\lambda_r = 0 \tag{4.19}$$

$$r_r i_{dr} + p\lambda_r = 0 \tag{4.20}$$

Thus from Equations 4.14 and 4.15 the rotor currents are derived as in Equations 4.21 and 4.22.

$$i_{qr} = \frac{-L_m}{L_r} i_{qs} \tag{4.21}$$

$$i_{dr} = \frac{\lambda_r - L_m i_{ds}}{L_r} \tag{4.22}$$

Substituting for d and q axes rotor currents from equations 4.21 and 4.22 into Equations 4.19 and 4.20 the following equations are obtained.

$$i_f = \frac{1}{L_m}[1 + T_r p]\lambda_r \tag{4.23}$$

$$\omega_{sl} = -\frac{r_r i_{qr}}{\lambda_r} = \frac{L_m}{T_r}\frac{i_T}{\lambda_r} \tag{4.24}$$

$$i_{T=} i_{qs} \tag{4.25}$$

$$i_{f=} i_{ds} \tag{4.26}$$

$$T_r = \frac{L_r}{r_r} \tag{4.27}$$

$$K_t = \frac{4}{3P} \tag{4.28}$$

Equation 4.23 resembles the field equation in a separately excited dc machine whose time constant is usually in the order of seconds. Substituting the rotor currents, the torque expression can be obtained as

$$T_e = \frac{3\mathrm{P}}{4}\frac{L_m}{L_r}(\lambda_{dr} i_{qs} - \lambda_{dr} i_{ds}) = \frac{3p}{4}\frac{L_m}{L_r}(\lambda_{dr} i_{qs}) = K_t\,(\lambda_r i_{qs}) \tag{4.29}$$

From Equation 4.29 it can be observed that torque is proportional to the product of the rotor flux linkages and the stator q-axis current. This resembles the air gap torque expression of the dc motor, which is proportional to the product of the field flux linkages and the armature current.

When the rotor flux linkage is kept constant, the torque becomes directly proportional to the torque-producing component of the stator current just like in a separately excited DC motor. Similar to the time constant seen in DC machines, which typically spans a few milliseconds, the torque current in an induction motor also responds within a comparable timeframe.

Equations 4.23 and 4.29 complete the transformation of the induction machine into an equivalent separately excited dc motor from control point of view. The stator current phasor is the sum of the 'd' and the 'q' axes stator currents in any reference frame given as

$$i_s = \sqrt{(i_{qs})^2 + (i_{ds})^2} \tag{4.30}$$

and the 'dq' axes to abc phase current relationship is obtained from Equation 4.4.

4.3.3. Implementation Of Indirect Vector Control

The indirect vector control method requires only the rotor speed as input from the machine, while all other parameters are estimated internally. The setup for implementing this control approach is illustrated in Figure 4.3. In this scheme, the torque command is typically derived from the speed error, which is processed using a PI controller. For simplicity, the flux reference is usually made dependent on the motor speed.

defined by

$$\lambda_r^* = \lambda_b \qquad 0 \leq |\omega_r| \leq \omega_{rated} \tag{4.31}$$

$$= \frac{\omega_b}{|\omega_r|}\lambda_b \quad \omega_b \leq |\omega_r| \leq \omega_{r(max)} \tag{4.32}$$

where λ_b and ω_r are the rated or the base rotor flux linkages and rotor speed respectively. The flux is kept at rated value up to rated speed; above that the flux is weakened to maintain the power output at a constant value.

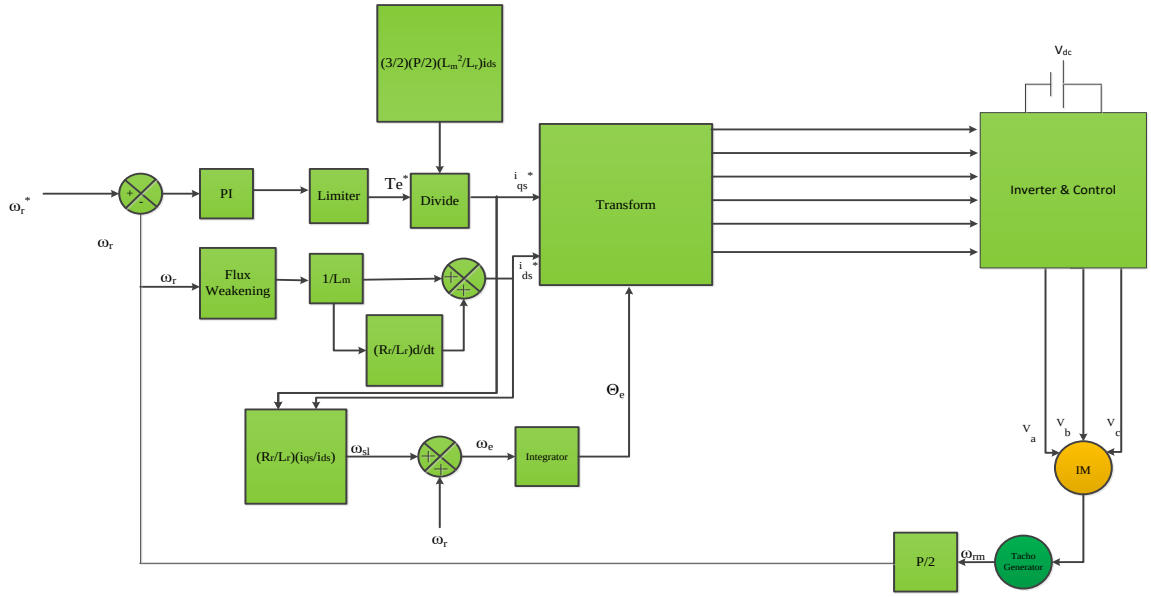

Figure 4.3: Implementation of the indirect vector control.

The current commands are processed using a power amplifier, which typically consists of a standard converter-inverter setup. The rotor position Θ_r is measured using an encoder, and this data is converted into a digital signal for feedback purposes. While the earlier explanation assumes a current source inverter for simplicity, this thesis uses a voltage source inverter (VSI). Therefore, the generated current references are translated into voltage commands and supplied to the VSI for implementation.

Table 4.1: Parameters of Three Phase Induction Motor (50 Hp)

Power	**50 Hp**
Poles	**4**
Voltage	**460 V**
Frequency(f)	**60 Hz**
R_s	**0.087Ω**
R_r	**0.228 Ω**
X_{Ls}	**0.302 Ω**
X_{Lr}	**0.302 Ω**
X_m	**13.02 Ω**
J	**1.662 kg-m^2**
T_L(rated)	**198 Nm**

4.4 Results and Observations:

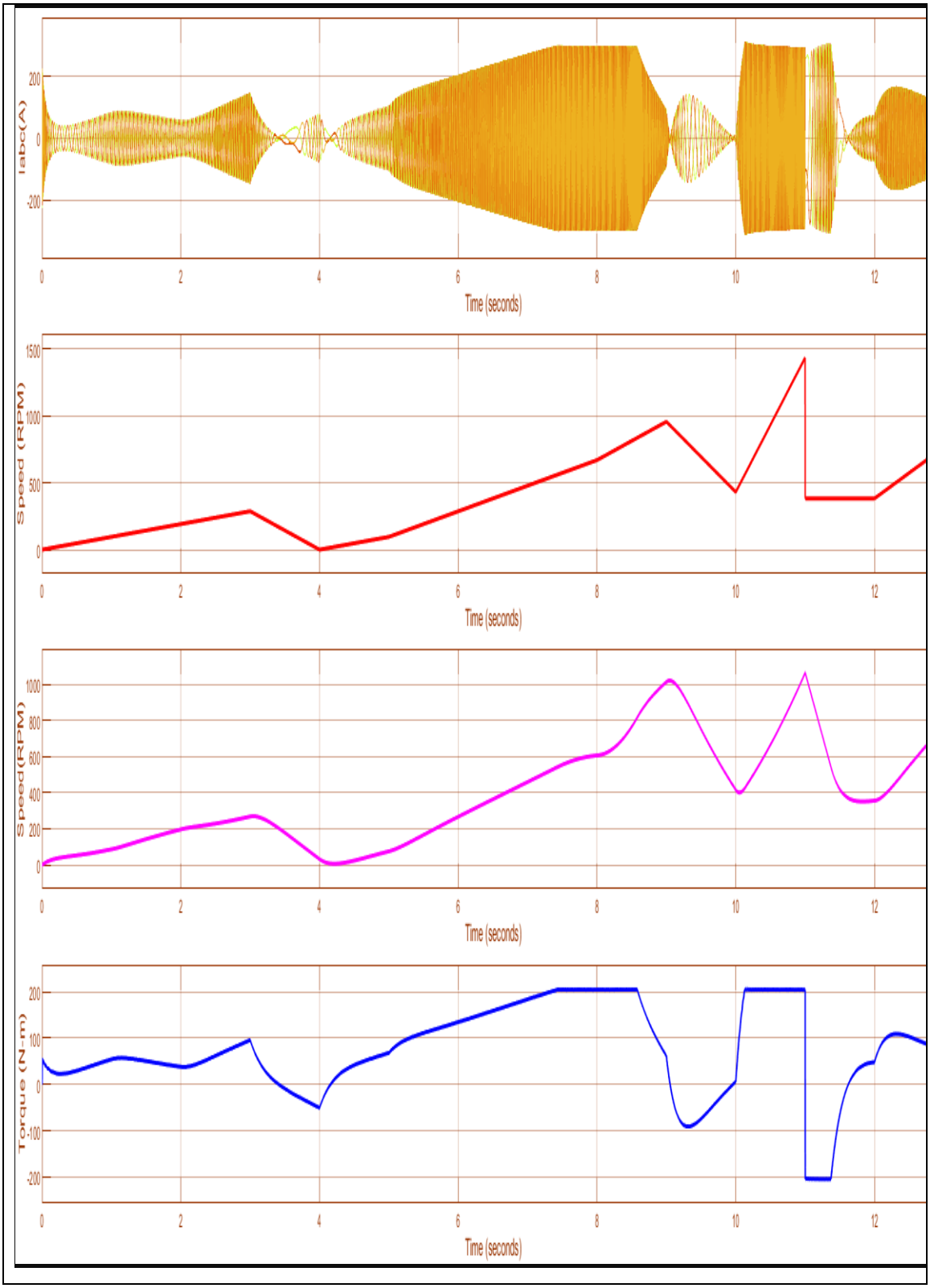

Figure 4.4: Simulation Results of FOC

1. Stator Currents

- The waveform amplitude varies over time, indicating modulation of torque and flux-producing components.
- As the torque demand increases, phase current amplitude increases, and vice versa.
- Currents become denser (higher frequency and amplitude) during high-torque/high-speed conditions, reflecting the inverter's PWM response to demand.

2. Reference Speed vs Actual Speed

- The actual speed tracks the reference speed effectively with minimal lag, confirming good dynamic performance of the speed control loop.
- Despite abrupt changes in reference (especially after 10s), the motor adapts quickly and smoothly.

3. Torque Response

- The torque plot shows variations corresponding to speed reference changes and load transitions.
- Some oscillations during sharp changes indicate system response delay, but the control remains stable and responsive.
- Torque goes negative temporarily, likely during regenerative braking or rapid deceleration.

4. Correlation Among Torque, Speed and Phase Currents

- When torque decreases, phase current amplitude also decreases confirming that the torque-producing component i_q is being regulated correctly.
- As speed demand increases, torque initially rises to accelerate the rotor, and this is reflected in a rise in current magnitude.

Chapter 5

CONTROL OF DUAL MOTORS WITH REDUNDANCY

CHAPTER 5

CONTROL OF DUAL MOTORS WITH REDUNDANCY

5.1 Introduction:

In this chapter, a new scheme is proposed to supply two three-phase induction motors using a single Five-Leg Inverter (FLI) by sharing one common leg. Motor 1 is controlled by adjusting its modulation index; however, due to the shared phase, any change in Motor 1's modulation also affects the input voltage of Motor 2. As a result, both motors operate smoothly and in balanced condition only when their modulation indices are equal. This chapter discusses in detail how to achieve independent control of both motors while maintaining a constant magnitude of the rotating magnetic field (RMF), ensuring stable and efficient performance.

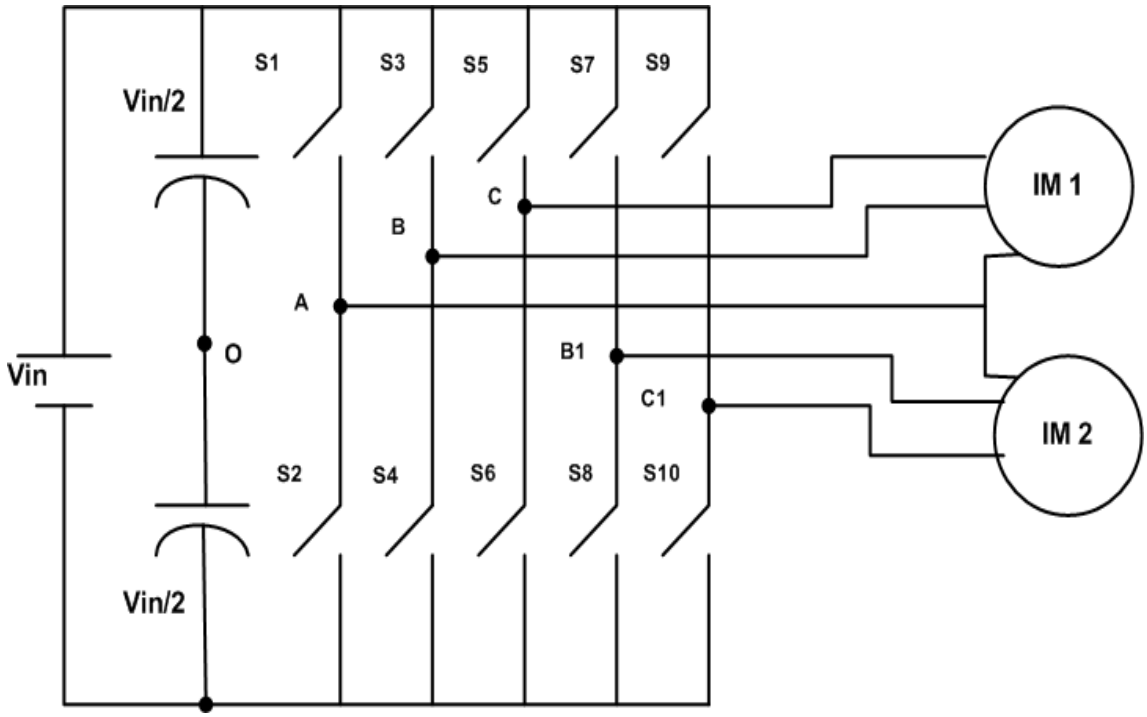

Figure 5.1 Block Diagram for The Proposed Scheme

Figure 5.1 illustrates block diagram of proposed scheme where two induction motors are connected to FLI

5.2 Balanced Five Phase Supply:

In five phase balanced supply each voltage is displaced by 72° and have constant magnitude.

$$V_a = V_m \sin(\omega t) \tag{5.1}$$

$$V_b = V_m \sin\left(\omega t - \frac{2\pi}{5}\right) \tag{5.2}$$

$$V_c = V_m \sin\left(\omega t - \frac{4\pi}{5}\right) \tag{5.3}$$

$$V_d = V_m \sin\left(\omega t - \frac{6\pi}{5}\right) \tag{5.4}$$

$$V_e = V_m \sin\left(\omega t - \frac{8\pi}{5}\right) \tag{5.5}$$

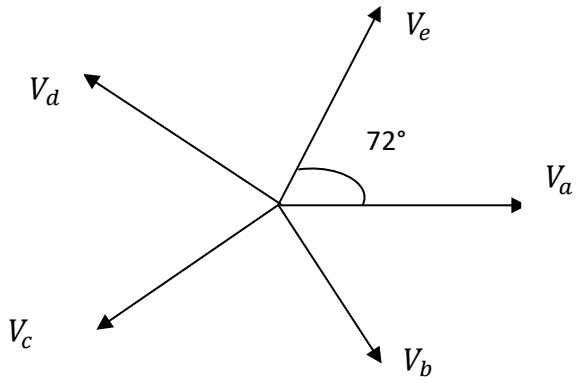

Figure 5.2 Five Phase balanced supply

Eq(5.1) to Eq(5.5) denoting five phase balanced supply. By keeping Va as common which has zero phase difference between two 3 phase motors as we are trying to produce constant rotating magnetic field (RMF) in both motors. By grouping a-c-e and a-b-d phase sequence and connecting in this manner in our both motors can be one of the solutions. But these sequences are unbalanced with respect to the motors and if connected without any changes it will produce distorted flux which in return give high torsional oscillations in the machine.

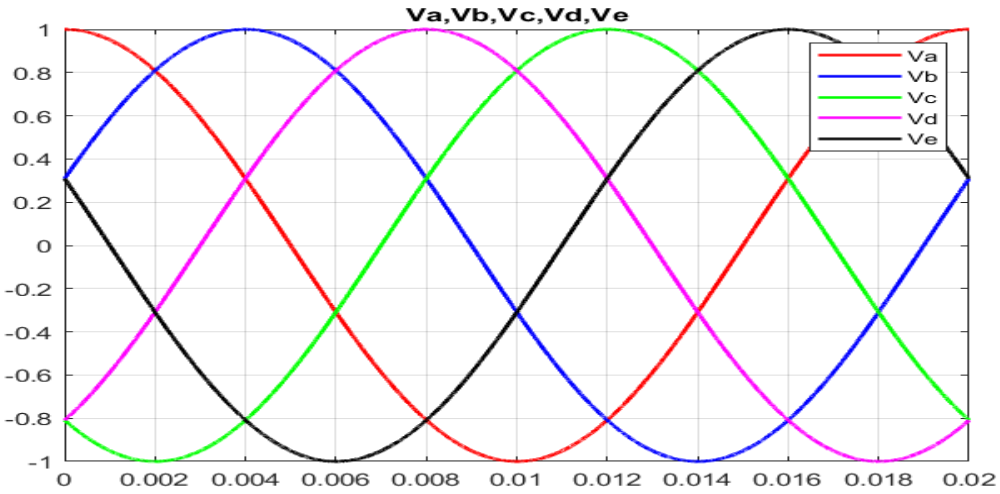

Figure 5.3 Waveform of five phase supply

Figure 5.3 illustrates waveform of balanced Five phase supply

When sequence is a-c-e for Motor 1 and sequence a-b-d for Motor 2, in a-c-e sequence magnitude will be equal but phase c is shifted from phases a and e by 144° and phase e shifted from phase a by 72° while considering phase a as reference phasor. Similarly in a-b-d sequence magnitude will be equal but phase c is shifted from phases a and b by 144° and phase b shifted from phase a by 72° while considering phase a as reference phasor.

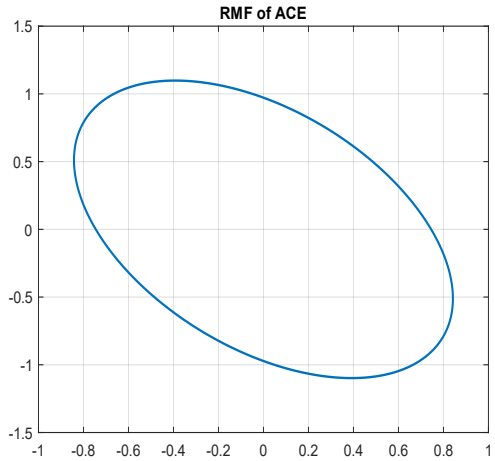

Figure 5.4 (a) RMF of actual ACE

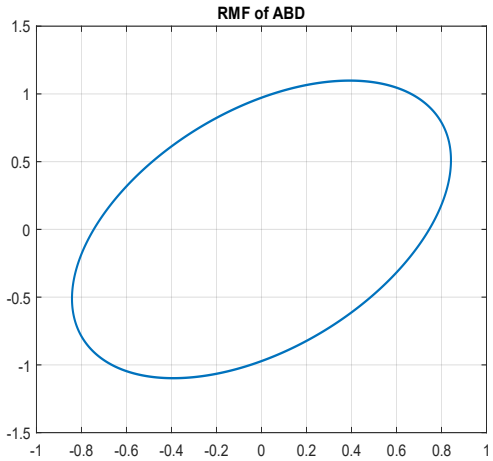

Figure 5.4(b) RMF of actual ABD

With above sequences RMF will look like given below in figure 5.4(a) and figure 5.4(b) which are distorted. As we can see that it is not perfect circle which means it has torsional

oscillations in other words magnitude of $v_\alpha and\ v_\beta$ is not same and there is no 90° displacement between them. So, in order to get rid of this situation above equations should be modified.

By considering a machine whose stator windings are displaced in space at an angle of 120° is supplied through a-c-e as shown in figure 5.5, then magnitudes of the phases other than phase a can be obtained as

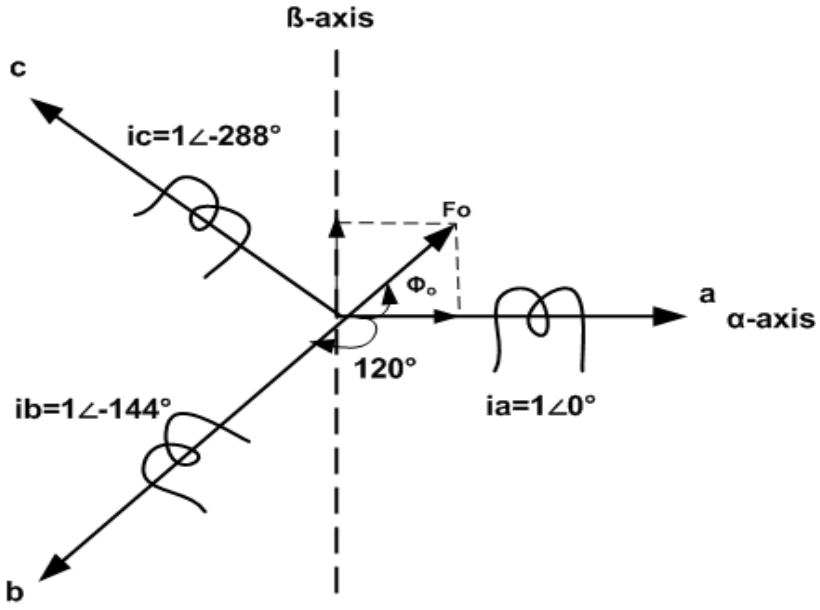

Figure 5.5 Balanced three phase winding supplied from ACE

Figure 5.5 illustrates when a-c-e sequence directly applied to the motor in which windings are 120° electrically apart .

Considering amplitude, A, B, C, D and E for V_a, V_b, V_c, V_d and V_e respectively.

$$V_a = A\ sin(\omega t) \tag{5.6}$$

$$V_b = B\ sin\left(\omega t - \frac{2\pi}{5}\right) \tag{5.7}$$

$$V_c = C\ sin\left(\omega t - \frac{4\pi}{5}\right) \tag{5.8}$$

$$V_d = D\ sin\left(\omega t - \frac{6\pi}{5}\right) \tag{5.9}$$

$$V_e = E\ sin\left(\omega t - \frac{8\pi}{5}\right) \tag{5.10}$$

Then by using Figure (5.5) and as V_a is the reference voltage then considering A=1 and a-c-e phase sequence we get: -

$$(1+j0)(1*\cos(\omega t)) + (-0.5 - j0.866)(C\cos(\omega t - 144°))$$

$$+ (-0.5 + j0.866)E(\cos(\omega t - 288°)) = F_o(\cos(\Phi_o) + j\sin(\Phi_o)) \quad (5.11)$$

Separating real and imaginary part of Eq. (5.11) and by solving we get equation in the form of:

$$\cos(\omega t)\, P - \sin(\omega t)\, Q = F_o \cos(\Phi_o) \quad (5.12)$$

$$\cos(\omega t)\, R + \sin(\omega t)\, S = F_o \sin(\Phi_o) \quad (5.13)$$

where,

$$P=0.5C\cos(144°)-0.5E\cos(288°) \quad (5.14)$$

$$Q=0.5C\sin(144°)-0.5E\sin(288°) \quad (5.15)$$

$$R=\frac{\sqrt{3}}{2}(-C\cos(144°)+0.5E\cos(288°)) \quad (5.16)$$

$$S=\frac{\sqrt{3}}{2}(-C\sin(144°)+0.5E\sin(288°)) \quad (5.17)$$

If P=S and Q=R, then the above, then Eq (5.14) to Eq (5.17) represents a circle which implies that RMF so formed by those equations is of constant magnitude and by solving above mentioned equations we get.

$C = -1.8271$ and E=1

Similarly, by doing the same process as a-c-e sequence for a-b-d sequence we get:

B =1 and $D = -1.8271$

Then by using above values modified five phase supply and modified RMF of a-c-e sequence and a-b-d sequence is shown below: Figure 5.6(a) and 5.6(b) illustrates RMF as perfect circle.

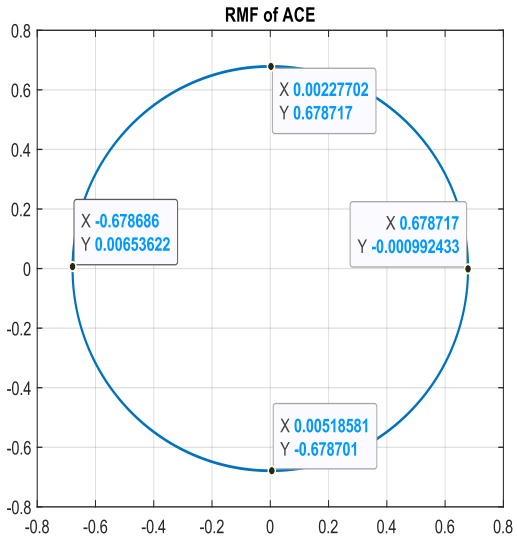

Figure 5.6 (a) RMF of Modified ACE

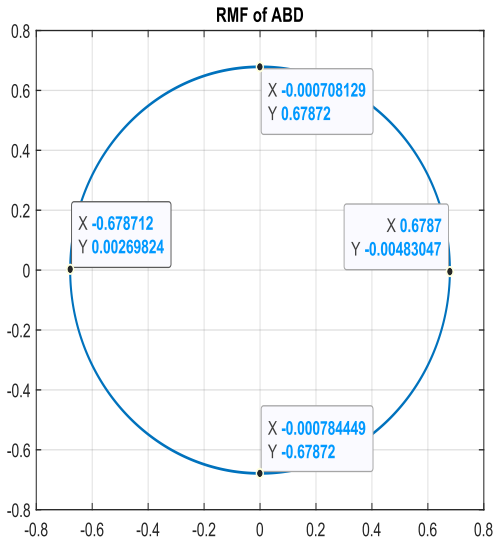

Figure 5.6 (b) RMF of Modified ABD

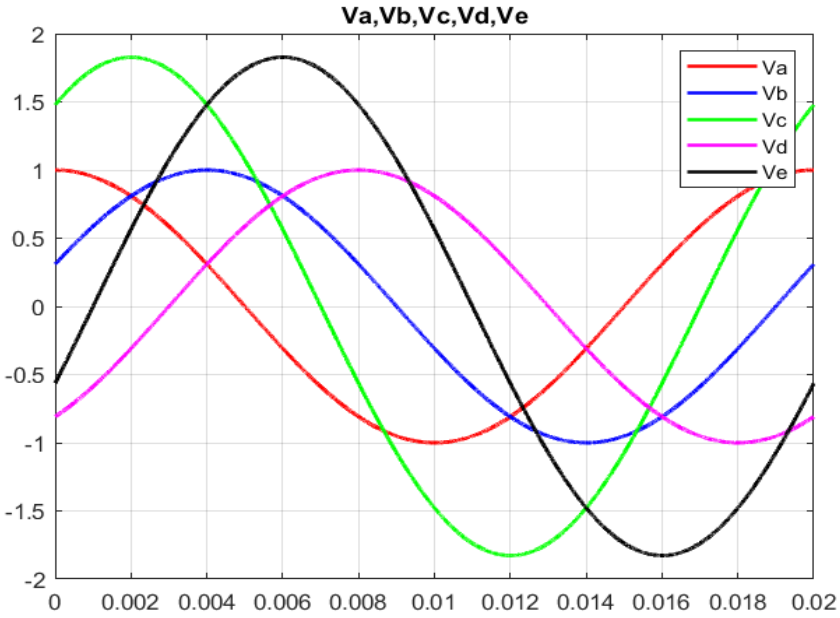

Figure 5.7 Modified Five Phase Supply

Figure 5.7 illustrates modified five phase supply which gives alpha beta voltage same in magnitude and 90° apart after Clarke's transformation.But with method the problem was high zero sequence voltage which is not feasible for the motor as shown in Figure 5.8. As Figure 5.8 shows alpha beta and zero voltages where zero voltages are 2 times in magnitude with respect to alpha and beta voltages.

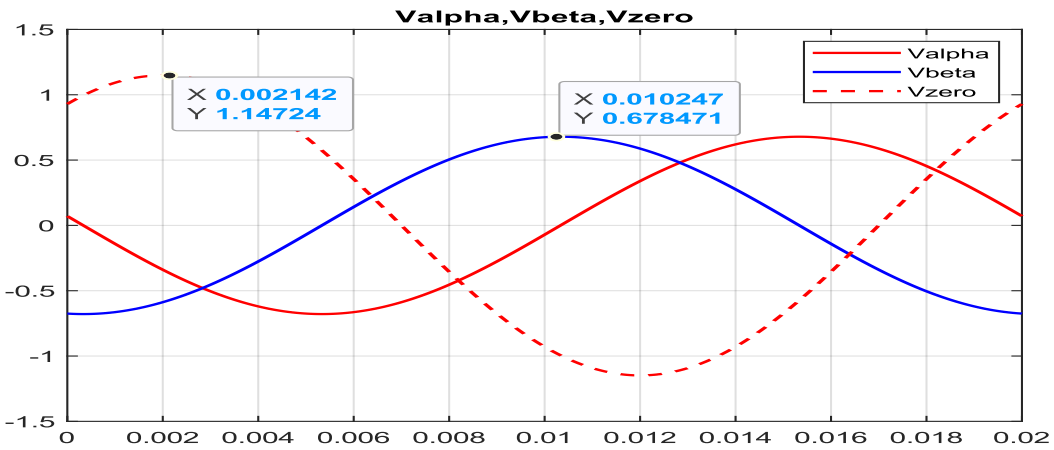

Figure 5.8 Alpha, Beta and Zero Voltages

But as motors are delta connected it will not have any effect because of it but for prolonged use it may cause heating and torque pulsations in the motor. So, to get rid of this problem another method is discussed in the later half.

5.3 Different Set of Phases

In a balanced n-phase supply, each phase voltage is equal in magnitude and symmetrically displaced in time. A Five-Leg Inverter (FLI) is leveraged to supply two three-phase induction motors using a shared DC bus and five switch legs. The first three legs (Leg A, B, and C) operate as a conventional three-phase voltage source inverter (VSI) and supply Motor 1. To supply Motor 2, the same Phase A leg is shared, assuming it as a reference with zero phase shift, while the remaining two phases (B_1 and C_1) are independently controlled using Leg D and Leg E, respectively.

$$V_a = A\,sin(\omega t) \tag{5.18}$$

$$V_b = A\,sin\left(\omega t - \frac{2\pi}{3}\right) \tag{5.19}$$

$$V_c = A\,sin\left(\omega t + \frac{2\pi}{3}\right) \tag{5.20}$$

$$V_{b1} = B\,sin(\omega t - \theta_b) \tag{5.21}$$

$$V_{c1} = B\,sin(\omega t - \theta_c) \tag{5.22}$$

Here A and B are amplitude of Motor 1 and Motor 2

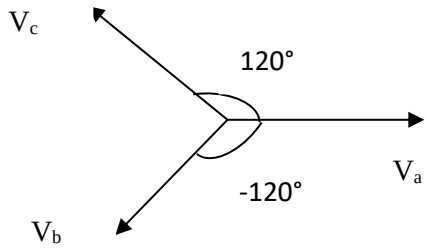

Figure (5.9(A)) Balanced Supply for Motor 1

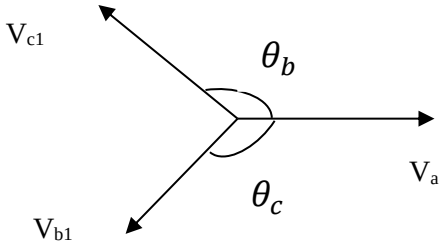

Figure (5.9(B)) Supply of Motor 2 Which Can Be Balanced as Well as Unbalanced

Figure (5.9(A)) represents the balanced supply for Motor 1 which has constant magnitude and 120° apart from each other but Figure (5.9(B)) represents the balanced as well as unbalanced supply for Motor 2 which adjust its phase difference accordingly so that it shows balanced behaviour.

5.4 Deriving B, Θ_b and Θ_c in terms of A

Considering A=0.75 (pu)

Then by Clarke's Transformation: -

$$\begin{bmatrix} v_\alpha \\ v_\beta \end{bmatrix} = \frac{2}{3}\begin{bmatrix} 1 & -\frac{1}{2} & -\frac{1}{2} \\ 0 & \frac{\sqrt{3}}{2} & -\frac{\sqrt{3}}{2} \\ \frac{1}{2} & \frac{1}{2} & \frac{1}{2} \end{bmatrix}\begin{bmatrix} v_a \\ v_b \\ v_c \end{bmatrix} \quad (5.23)$$

Therefore,

$$v_\alpha = \frac{2}{3}\left(v_a - \frac{v_b}{2} - \frac{v_c}{2}\right) \quad (5.24)$$

$$v_\beta = \frac{2}{3}\left(\frac{\sqrt{3}v_b}{2} - \frac{\sqrt{3}v_c}{2}\right) \quad (5.25)$$

As this system is balanced v_0 is zero.

As v_a, v_b, v_c are instantaneous voltages.

Therefore, $v_a = 0.75\angle 0°, v_b = 0.75\angle -120°, v_c = 0.75\angle 120°$ (5.26)

By substituting Eq (5.26) in Eq (5.24) and Eq (5.25) and solving it

We get,

$$v_\alpha = 0.75 \quad (5.27)$$

$$v_\beta = j0.75 \quad (5.28)$$

Here ‘j’ is the imaginary unit.

As we want our Motor 2 to show the same behavior as that of Motor 1 when it has magnitude of 0.75, then by using above equation we get:

Substituting Eq (5.27) and Eq (5.28) in Eq (5.24) and Eq (5.25)

$$0.75 = \frac{2}{3}\left(v_a - \frac{v_b}{2} - \frac{v_c}{2}\right) \tag{5.29}$$

$$j0.75 = \frac{2}{3}\left(\frac{\sqrt{3}v_b}{2} - \frac{\sqrt{3}v_c}{2}\right) \tag{5.30}$$

For Motor 2:

$$v_a = A\angle 0°, v_b = B\angle\theta_b, v_c = B\angle\theta_c \tag{5.31}$$

Here, θ_b and θ_c are in degrees.

Substituting Eq(5.31) in Eq (5.29) and Eq (5.30) we get

$$0.75 = \frac{2}{3}\left(A - \frac{B\angle\theta_b}{2} - \frac{B\angle\theta_c}{2}\right) \tag{5.32}$$

$$j0.75 = \frac{2}{3}\left(\frac{\sqrt{3}B\angle\theta_b}{2} - \frac{\sqrt{3}B\angle\theta_c}{2}\right) \tag{5.33}$$

From Eq (5.32) and Eq (5.33) we get

$$A - 1.125 = \frac{B\angle\theta_b}{2} + \frac{B\angle\theta_c}{2} \tag{5.34}$$

$$j1.3 = B\angle\theta_b - B\angle\theta_c \tag{5.35}$$

By solving Eq. (5.34) and Eq. (5.35)

We get:

$$B\angle\theta_b = A - 1.125 + j0.65 \tag{5.36}$$

Similarly,

$$B\angle\theta_c = A - 1.125 - j0.65 \tag{5.37}$$

Here in Eq (5.36) and Eq (5.37) real part is $A - 1.125$ and imaginary part is 0.65 and -0.65 respectively.

As Eq (5.36) and Eq (5.37) is in cylindrical form converting it into polar form we get:

$$\boldsymbol{B = \sqrt{(A - 1.125)^2 + (0.65)^2}} \tag{5.38}$$

$$\boldsymbol{\theta_b = \tan^{-1}\left(\frac{0.65}{A - 1.125}\right)} \tag{5.39}$$

$$\boldsymbol{\theta_c = \tan^{-1}\left(\frac{-0.65}{A - 1.125}\right)} \tag{5.40}$$

5.5 Results and Conclusion:

5.5.1Case 1: When A=B=0.75 then $\theta_b = 120°$ and $\theta_c = -120°$

Sr No.	Motor 1	Motor 2
1.	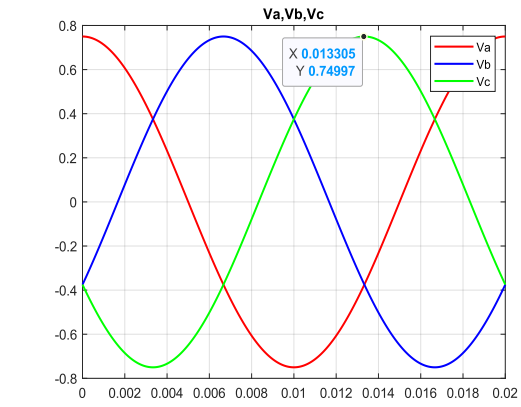	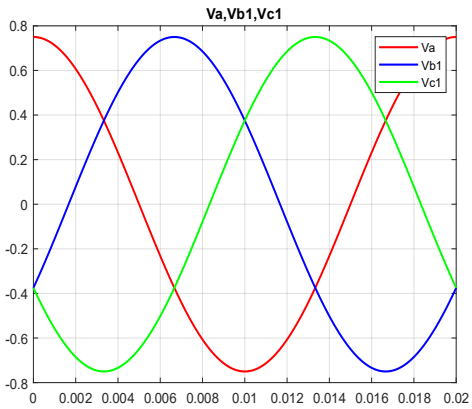
2.	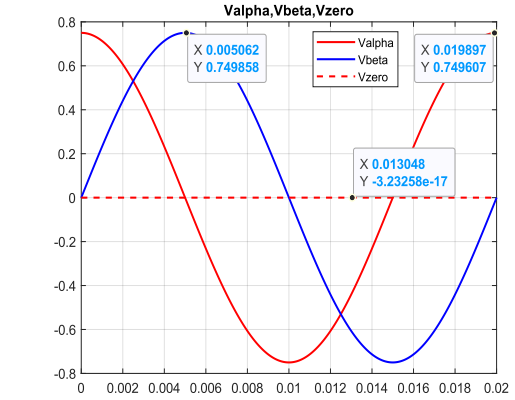	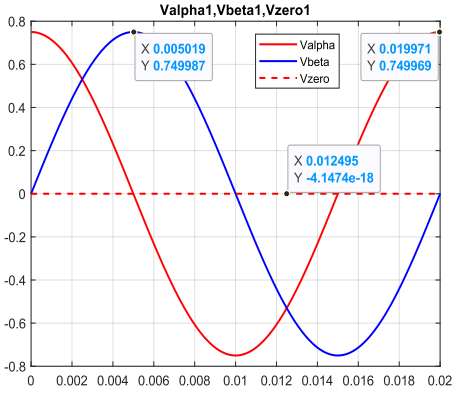
3.	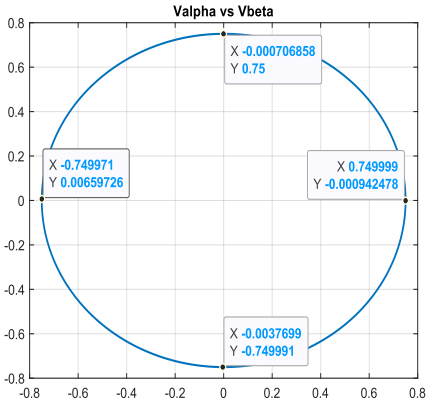	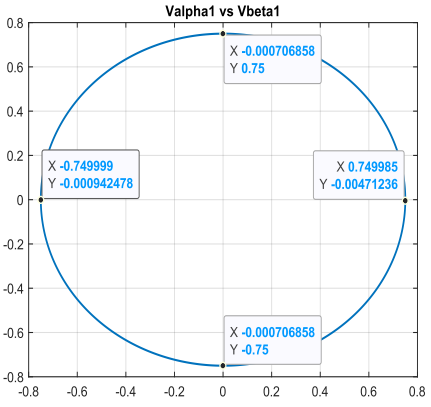

Figure 5.10 (a) (i)Phase Voltages (ii)V_{alpha},V_{beta} and V_{zero} (iii)RMF of Motor 1 and Motor 2 respectively when A=0.75

5.5.2 Case 2: When A= 0.5 then B=0.9017, $\theta_b = 133.87°$ and $\theta_c = -133.87°$

Sr No.	Motor 1	Motor 2
1.	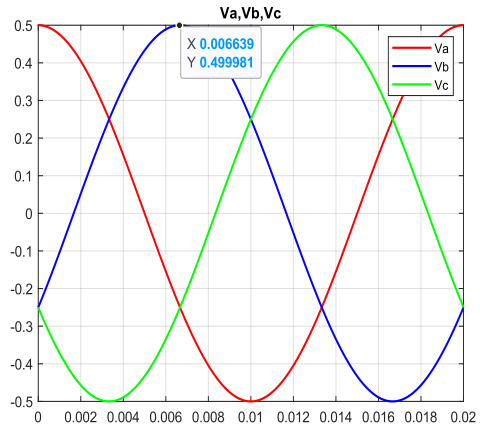	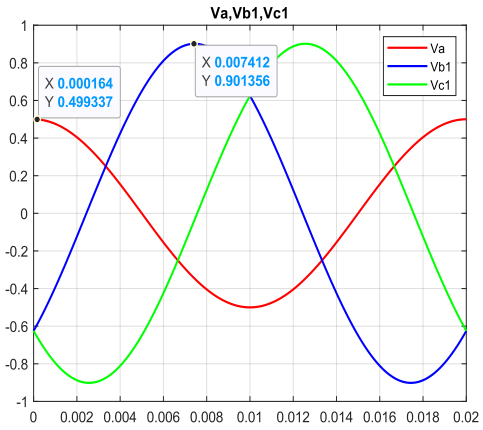
2.	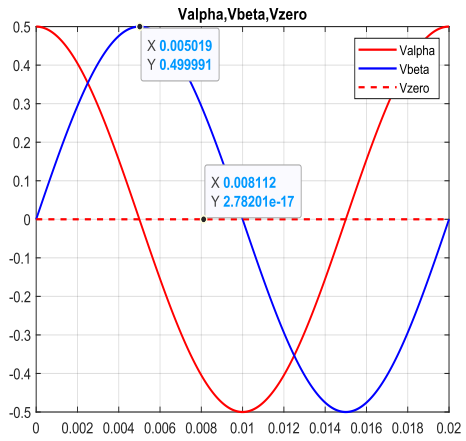	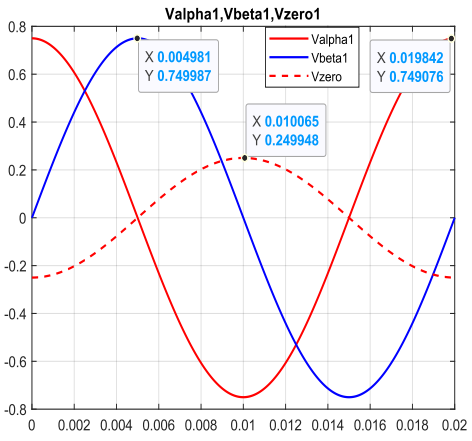
3.	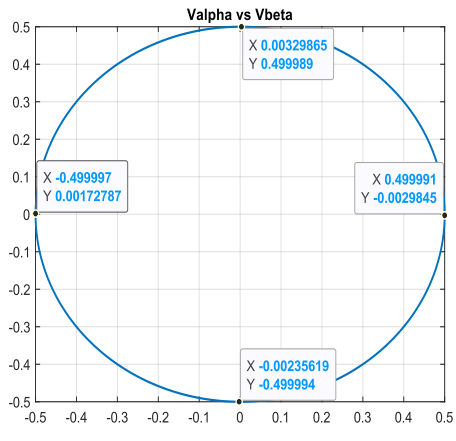	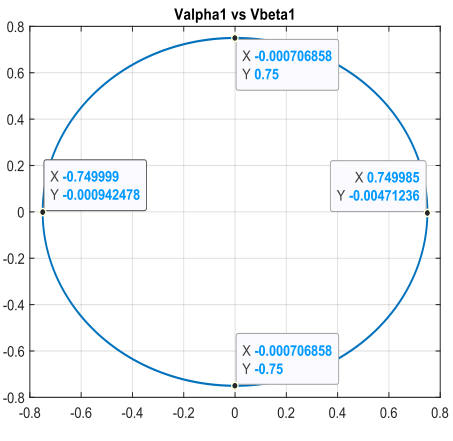

Figure 5.10 (b) (i)Phase Voltages (ii)V_{alpha},V_{beta} and V_{zero} (iii)RMF of Motor 1 and Motor 2 respectively when A=0.5

5.5.3 Case 3: When A= 0.65 then B=0.8050, $\theta_b = 126.158°$ and $\theta_c = -126.158°$

Sr No.	Motor 1	Motor 2
1.	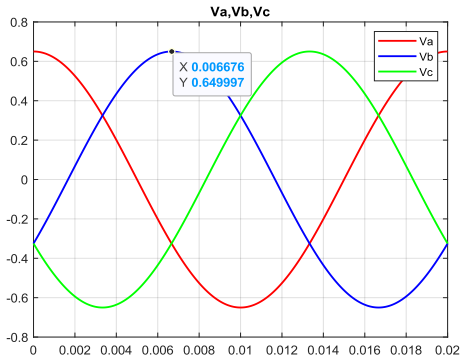	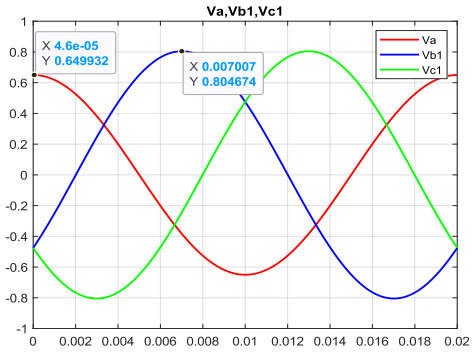
2.	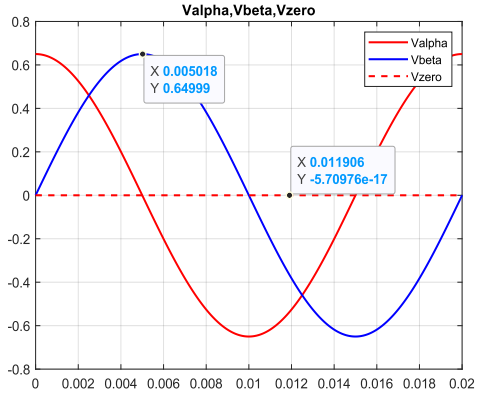	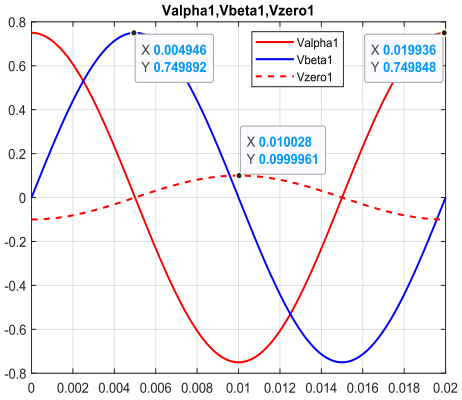
3.	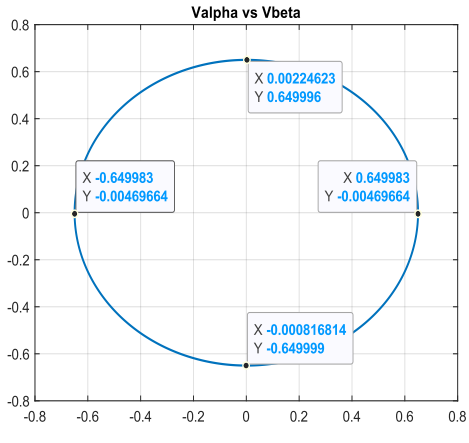	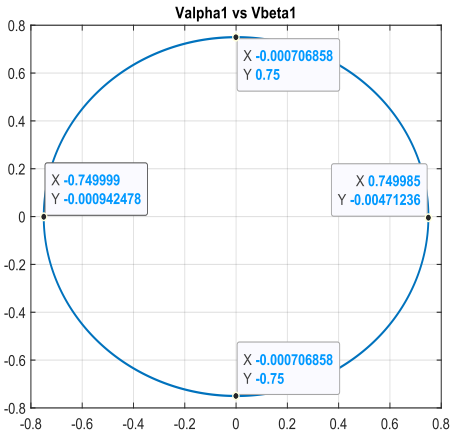

Figure 5.10 (c) (i)Phase Voltages (ii)V_{alpha},V_{beta} and V_{zero} (iii)RMF of Motor 1 and Motor 2 respectively when A=0.65

5.5.4 Case 4: When A= 0.85 then B=0.70578, $\theta_b = 112.932°$ and $\theta_c = -112.932°$

Sr No.	Motor 1	Motor 2
1.	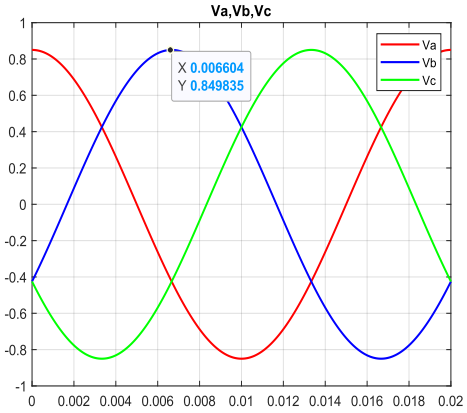	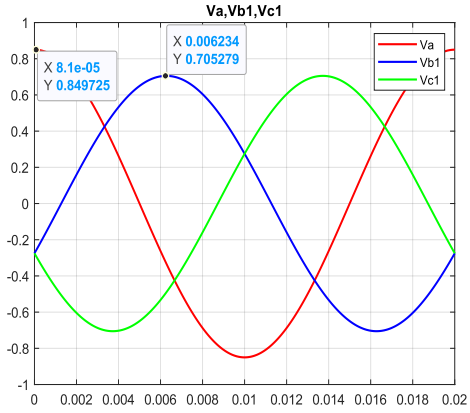
2.	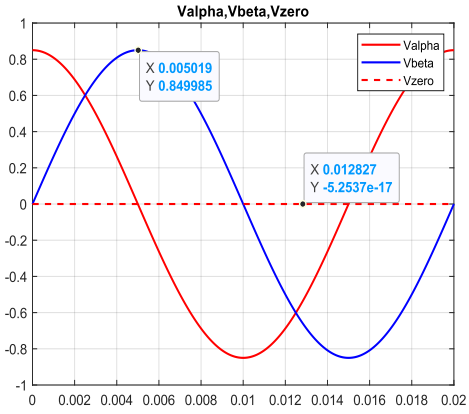	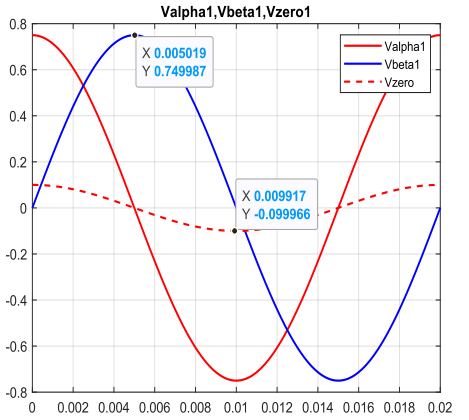
3.	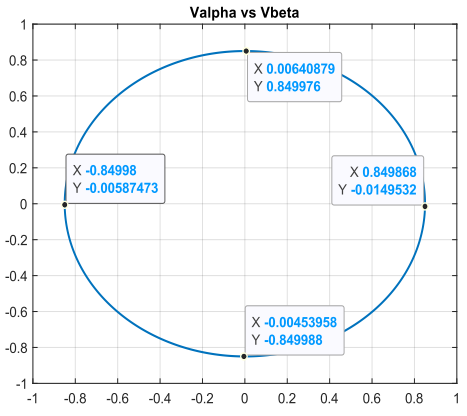	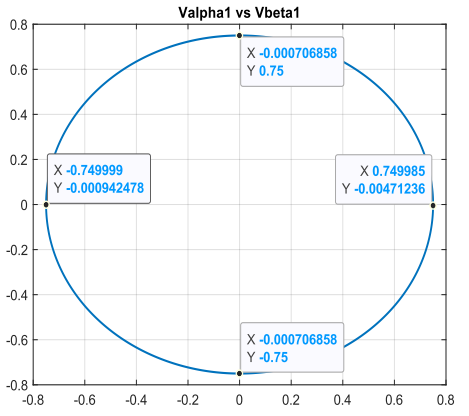

Figure 5.10 (d) (i)Phase Voltages (ii)V_{alpha},V_{beta} and V_{zero} (iii)RMF of Motor 1 and Motor 2 respectively when A=0.85

5.5.5 Case 5: When A= 1 then B=0.6619, $\theta_b = 100.8855°$ and $\theta_c = -100.8855°$

Sr No.	Motor 1	Motor 2
1.	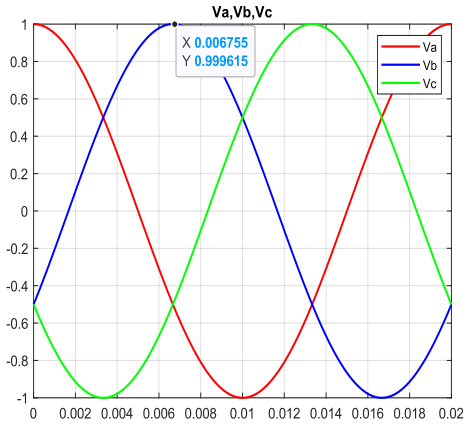	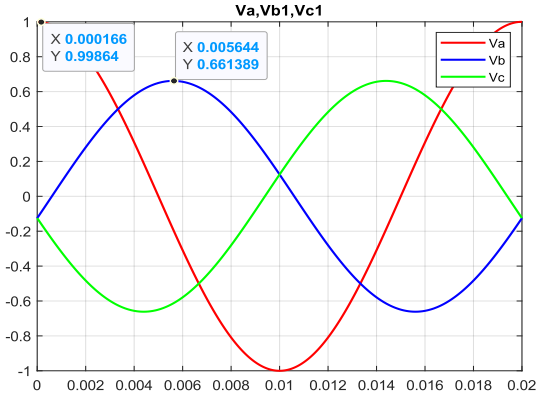
2.	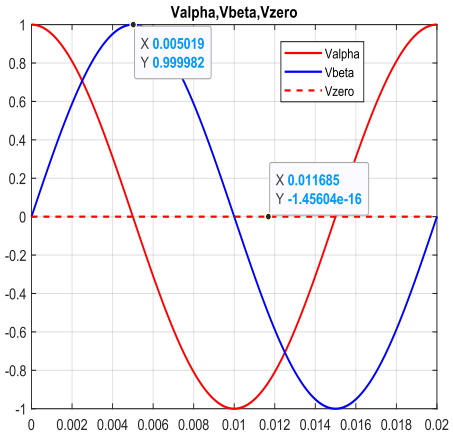	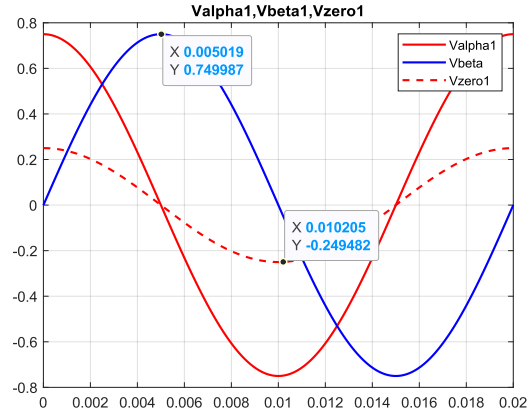
3.	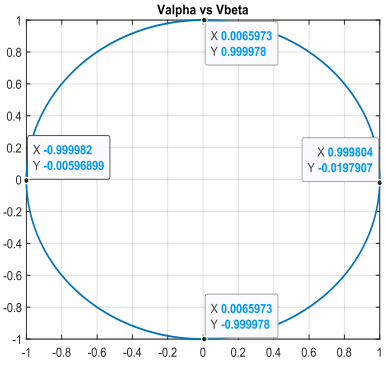	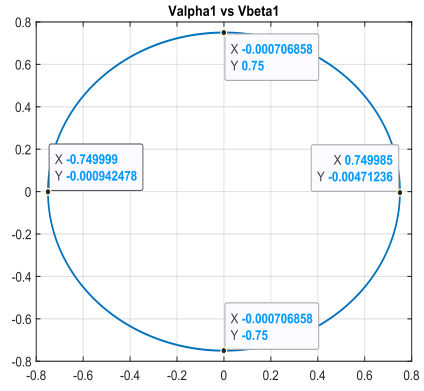

Fig. 5.10 (e) (i)Phase Voltages (ii)V_{alpha},V_{beta} and V_{zero} (iii)RMF of Motor 1 and Motor 2 respectively when A=1

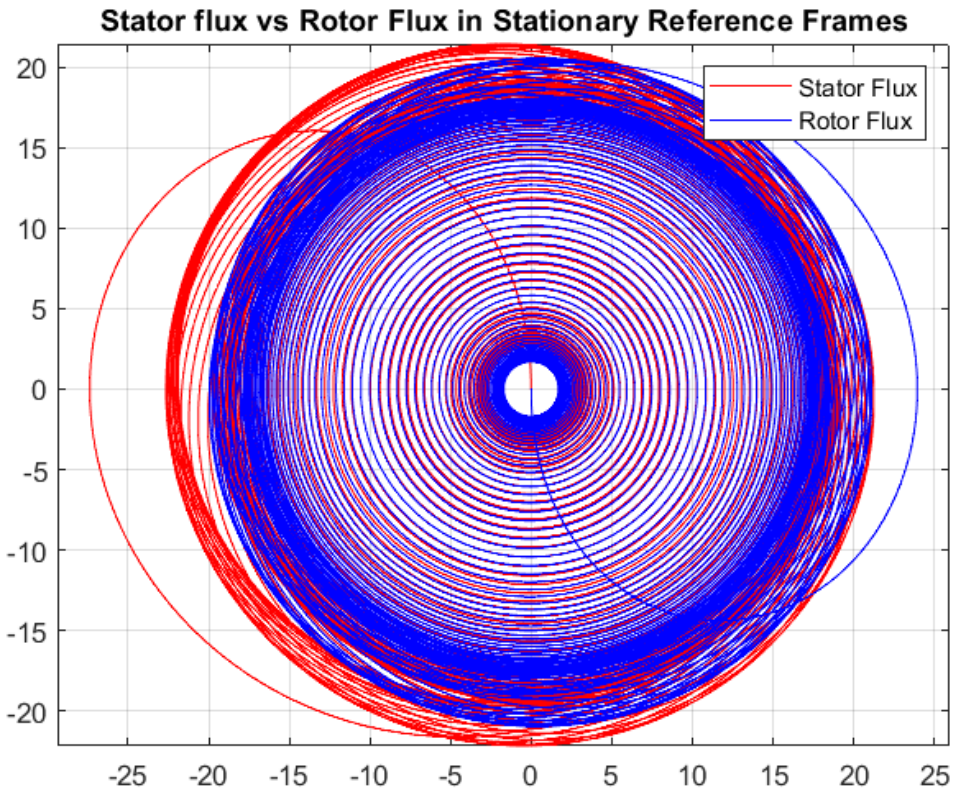

Figure 5.11 Stator Flux Vs Rotor Flux in Stationary Reference Frame

Figure 5.10(a) to Figure 5.10(e) all the cases are showed for both motor 1 and motor 2 .And it should be noted that when Motor 1 is changing Motor 2 is not changing its behaviour.

Figure 5.11 shows RMF is showing balanced characteristics in motor 2 when voltages are unbalanced as mentioned in all the cases mentioned above and it is done on the 50 Hp motor which is at 50 N-m load for other parameters refer table 4.1.

In the analysis presented in Figures 5.2(a) through 5.2(e), a modulation index of 0.75 is selected as a representative value within the linear operating range of Space Vector Pulse Width Modulation (SVPWM). This choice is strategic, considering that SVPWM allows modulation indices from 0 up to approximately 1.154 when third harmonic injection is employed. However, to maintain operation within the linear modulation region and avoid the complexities associated with overmodulation, it's practical to limit the modulation index to a maximum of 1. Selecting 0.75, the average of 0.5 and 1, provides a balanced

operating point that offers sufficient headroom for Motor 1 to vary its modulation index without entering the overmodulation region.

As the modulation index increases beyond 0.75, it's important to note that the zero-sequence voltage component also increases. This component can reach amplitudes approximately 33% of the resultant phase voltages, as observed in Figures 5.2(b) and 5.2(e). Elevated zero-sequence voltages can lead to unbalanced phase voltages, adversely affecting motor performance and potentially causing additional losses or stress on the motor windings.

Therefore, it's advisable to operate Motor 1 with modulation indices close to 0.75. This is corroborated by Figures 5.2(c) and 5.2(d), where modulation indices of 0.65 and 0.85, respectively, result in negligible zero-sequence voltage components. Maintaining the modulation index within this range ensures balanced phase voltages and optimal motor performance.

In summary, selecting a modulation index around 0.75 for Motor 1 strikes a balance between operational flexibility and the minimization of zero-sequence voltage effects, thereby enhancing the overall stability and efficiency of the motor control system.

Chapter 6

CONCLUSION AND FUTURE SCOPE

CHAPTER-6

CONCLUSION AND FUTURE SCOPE

6.1 Conclusion

In this thesis, in Chapter.2 Dynamic Modelling of 3 phase IM where Both sets of results complement each other and confirm the dynamic model's validity, The torque-speed profile reflects the effects of initial flux buildup and EMF, while the current waveforms demonstrate how these effects manifest electrically, The settling of currents aligns with the mechanical stabilization ,showing a complete dynamic response from startup to steady-state and The rotor current reversal and phase current overshoot confirm electromagnetic transients and back EMF effects during flux establishment.

In Chapter. 3 Space Vector Pulse Width Modulation (SVPWM) is an advanced and efficient technique for controlling voltage source inverters, offering better DC bus utilization, lower harmonic distortion, and reduced switching losses compared to traditional PWM methods. Its vector-based approach ensures smooth motor operation and precise control, making it ideal for high-performance applications. SVPWM is well-suited for implementation in both three-phase and multiphase systems, playing a key role in modern vector-controlled and multi-motor drive systems.

In Chapter 4. FOC of 3 phase IM where The FOC strategy successfully decouples torque and flux control, mimicking the performance of a separately excited DC motor.

In Chapter.5 Control of Dual Motor with redundancy in this proposed scheme where both motors are running independent of each other as phase of Motor 1 is varying with respect to modulation index other motor remains constant irrespective of the value of modulation index of Motor 1.

6.2 Future Scope

The proposed control scheme enables independent regulation of two machines while mitigating torsional oscillations. This approach can be integrated with both Field-Oriented Control (FOC) and Direct Torque Control (DTC), allowing one motor to operate at variable torque and speed while the other remains constant.

However, as detailed in Chapter 5, when the modulation index or phase voltage amplitude of Motor 1 varies, it introduces unbalanced supply voltages. To replicate the characteristics of balanced phase voltages—where phase voltages are 120° apart—using Space Vector Pulse Width Modulation (SVPWM), an advanced SVPWM technique is required. Conventional SVPWM is designed for balanced supply conditions and may not effectively handle unbalanced scenarios.

Advanced SVPWM methods, such as those based on vector space decomposition, offer enhanced flexibility by exploiting additional degrees of freedom in multi-phase systems. These techniques can reduce common-mode voltage and accommodate unbalanced conditions more effectively than traditional SVPWM approaches. Implementing such advanced modulation strategies ensures consistent performance and stability in systems experiencing supply voltage unbalances.

REFERENCES

[1] F. Blaschke, "The principle of field orientation as applied to the new transvector closed-loop control system for rotating-field machines," *Siemens Review*, vol. 34, no. 5, pp. 217–220, 1972.

[2] K. Hasse, "On the dynamic model of the induction motor," *Archiv für Elektrotechnik*, vol. 55, pp. 103–109, 1973.

[3] B. K. Bose, *Modern Power Electronics and AC Drives*. Upper Saddle River, NJ, USA: Prentice Hall, 2002.

[4] W. Leonhard, *Control of Electrical Drives*, 3rd ed. Springer, 2001.

[5] R. Krishnan, *Electric Motor Drives: Modeling, Analysis, and Control*. Upper Saddle River, NJ, USA: Pearson Education, 2001.

[6] P. Vas, *Vector Control of AC Machines*. Oxford, U.K.: Oxford Univ. Press, 1990.

[7] A. M. Trzynadlowski, *Introduction to Modern Power Electronics*, 2nd ed. Hoboken, NJ, USA: Wiley, 2010.

[8] J. Holtz, "Sensorless control of induction motor drives," *Proc. IEEE*, vol. 90, no. 8, pp. 1359–1394, Aug. 2002.

[9] E. Levi, "Multiphase electric machines for variable-speed applications," *IEEE Trans. Ind. Electron.*, vol. 55, no. 5, pp. 1893–1909, May 2008.

[10] A. H. M. A. Rahim, M. M. Islam, and M. Hossain, "Multiphase drive systems: Technologies and topologies," *Electr. Power Syst. Res.*, vol. 120, pp. 135–147, Mar. 2015.

[11] J. A. Ortiz-Rodriguez, E. Levi, and M. Jones, "Control of multiphase motor drives using vector space decomposition," *IEEE Trans. Ind. Electron.*, vol. 59, no. 10, pp. 4048–4056, Oct. 2012.

[12] M. Božić, E. Levi, M. Jones, and V. Biagini, "A five-phase inverter supplying two three-phase machines," *IEEE Trans. Ind. Electron.*, vol. 64, no. 2, pp. 1161–1170, Feb. 2017.

[13] R. Bojoi, F. Profumo, A. Tenconi, and K. J. Tseng, "Multiphase drives for automotive applications," *IEEE Ind. Electron. Mag.*, vol. 2, no. 1, pp. 6–16, Mar. 2008.

[14] L. Xu and D. Cheng, "A novel vector control scheme for dual-motor systems fed by a five-phase VSI," *IEEE Trans. Ind. Appl.*, vol. 46, no. 2, pp. 740–748, Mar./Apr. 2010.

[15] J. F. Gieras, *Advancements in Electric Machines*. Dordrecht, The Netherlands: Springer, 2008.

[16] M. Bongiorno, J. Svensson, and C. Sadarangani, "Generalized transformations for multiphase machines: Derivation, implementation, and validation," *IEEE Trans. Ind. Electron.*, vol. 58, no. 7, pp. 2479–2488, Jul. 2011.

[17] P. C. Krause, O. Wasynczuk, S. D. Sudhoff, and S. Pekarek, *Analysis of Electric Machinery and Drive Systems*, 3rd ed. Piscataway, NJ, USA: IEEE Press, 2013.

[18] S. J. Chapman, *Electric Machinery Fundamentals*, 5th ed. New York, NY, USA: McGraw-Hill, 2011.

[19] A. E. Fitzgerald, C. Kingsley, and S. D. Umans, *Electric Machinery*, 7th ed. New York, NY, USA: McGraw-Hill, 2013.

[20] T. Wildi, *Electrical Machines, Drives, and Power Systems*, 6th ed. Pearson, 2006.

[21] P. Pillay and R. Krishnan, "Modeling of induction machines for electric drives," *IEEE Trans. Ind. Appl.*, vol. 25, no. 6, pp. 985–996, Nov./Dec. 1989.

[22] D. G. Holmes and T. A. Lipo, *Pulse Width Modulation for Power Converters: Principles and Practice*. Piscataway, NJ, USA: IEEE Press, 2003.

[23] M. Jones, E. Levi, and M. Duran, "A review of space vector modulation techniques for multiphase inverter-fed drive systems," *IEEE Trans. Ind. Electron.*, vol. 63, no. 9, pp. 5442–5454, Sep. 2016.

[24] B. Wu, *High-Power Converters and AC Drives*. Hoboken, NJ, USA: Wiley-IEEE Press, 2006.

[25] J. Holtz, "Pulsewidth modulation – A survey," *IEEE Trans. Ind. Electron.*, vol. 39, no. 5, pp. 410–420, Oct. 1992.

[26] H. Abu-Rub, A. Iqbal, and J. Guzinski, *High Performance Control of AC Drives with MATLAB/Simulink Models*. Hoboken, NJ, USA: Wiley, 2012.

[27] B. K. Bose, *Power Electronics and Motor Drives: Advances and Trends*. Burlington, MA, USA: Academic Press, 2006.

[28] P. Vas, *Sensorless Vector and Direct Torque Control*. Oxford, U.K.: Oxford Univ. Press, 1998.

[29] J. Holtz, "Advanced motion control: It's time to think digital," *IEEE Ind. Electron. Mag.*, vol. 1, no. 1, pp. 7–18, Mar. 2007.

[30] Y. Zhang and J. Zhu, "Direct torque control of permanent magnet synchronous motor with reduced torque ripple and commutation frequency," *IEEE Trans. Power Electron.*, vol. 26, no. 1, pp. 235–248, Jan. 2011.

[31] A. M. Trzynadlowski, *The Field Orientation Principle in Control of Induction Motors*. Norwell, MA, USA: Kluwer Academic, 1994.

[32] D. Dujic, N. Bianchi, F. Profumo, and E. Levi, "High-performance control of multiphase machines with modular inverter topology," *IEEE Trans. Ind. Electron.*, vol. 55, no. 5, pp. 1946–1954, May 2008.

[33] L. Zhang, X. Zhang, and Y. Li, "Dual-motor independent vector control based on hybrid modulation with a single inverter," *IEEE Trans. Power Electron.*, vol. 33, no. 4, pp. 3240–3251, Apr. 2018.

[34] M. Jones, E. Levi, and N. Bianchi, "Control strategies for dual three-phase induction motor drives fed from a single VSI supply," *IEEE Trans. Ind. Electron.*, vol. 56, no. 6, pp. 2048–2056, Jun. 2009.

[35] E. Levi, "Advances in converter control and drive technology for multiphase machines," *Proc. IEEE*, vol. 105, no. 6, pp. 1034–1053, Jun. 2017.

[36] S. Williamson and A. C. Smith, "Pulsating torque and losses in multiphase induction motors," *IEEE Trans. Ind. Appl.*, vol. 39, no. 4, pp. 986–993, Jul./Aug. 2003.

[37] D. H. Bradley and S. Bolognani, "Trends in electrical drives: Challenges and research opportunities," *IEEE Ind. Electron. Mag.*, vol. 10, no. 4, pp. 56–67, Dec. 2016.

[38] R. Bojoi and L. R. Limongi, "Fault-tolerant control for multiphase motor drives with redundant phase legs," *IEEE Trans. Ind. Electron.*, vol. 63, no. 1, pp. 270–280, Jan. 2016.

[39] M. Jones, "Multimotor drives: Present applications and future trends," *IEEE Ind. Appl. Mag.*, vol. 21, no. 4, pp. 10–17, Jul./Aug. 2015.